QBithm: towards the coherent control of robust spin qubits in quantum algorithms

L. Escalera-Moreno[1]*

[1] *Max Planck Institut für Quantenoptik (MPQ), Garching bei München, Germany*

*luis.escalera.moreno@mpq.mpg.de

Abstract

Many efforts have succeeded over the last decade at lengthening the timescale in which spin qubits loss quantum information under free evolution. With these design principles, it is now timely to zoom out and take the whole picture: concerning applications that require user-driven evolutions, qubits should be assessed within the desired algorithm. This means to test qubits under external control while relaxation is active, and to maximize the algorithm fidelity as the actual figure of merit. Herein, we pose and analytically solve a master equation devised to run one-spin-qubit algorithms subject to relaxation. It is handled via a code, QBithm, which inputs gate sequences and relaxation rates thus connecting with the longstanding work devoted to their *ab initio* computation. We calculate fidelities against relaxation and imperfections, and implement well-known pulse sequences quantitatively agreeing with experimental data. Hopefully, this work will stimulate the study of many-qubit systems driven under relaxation and imperfections in quantum algorithms.

Introduction

Quantum simulation and quantum computation are expected to circumvent the exponential scaling that makes problems of wide interest -but with a large input- be unsolvable on classical computers. Instances of these problems include the prediction of materials relevant for industry and society, and the resolution of both optimization and combinatorics queries for policy-making. While this picture seems promising even at establishing new scientific and technological revolutions, the required experimental techniques rely on noisy operations that eventually spoil quantum information. A clear path towards a prototype able to solve all the above-mentioned problems in the mid term is nowadays elusive. Until quantum error correction protocols can be implemented in the lab on a massive scale, the provisory solution is that of operating on noisy intermediate-scale quantum (NISQ) devices. These are the platforms currently devoted to test algorithms with quantum advantage, [1] namely the ones which, by exploiting quantum properties, offer a more efficient scaling for those specific tasks where any conceivable classical algorithm would never do any better than exponentially. [2]

The logical operations or gates that compose a quantum algorithm are mapped onto manipulations of a given physical degree of freedom: the ground energy spectrum of an atom or an ion, the charge or the flux of a carrier, the polarization of a photon, or the motion of a mechanical oscillator. [3–6] In particular, beside technological applications such as sensing and communication, [7,8] the spin is one of the best-suited candidates for quantum computation, [9] where the minimum amount of information -termed as qubit- is physically realized in the spin states of defect centers, [10–12] donor atoms in silicon, [13], and magnetic molecules. [14–21] The proved potential of this degree of freedom in terms of initialization, long-lived coherent control, readout, single-spin manipulation, scalability and applications can be further enhanced within the molecular approach, where the well-developed tools of synthetic chemistry are ideal to tune and improve *at will* the properties of the so-called molecular spin qubits embedded in magnetic molecules. [22–43]

An important conundrum faced over the last decade from both the theoretical and the experi-

mental side has been to unveil those mechanisms that promote relaxation in a spin under free evolution. [44–46] In particular, this has been crucial to deepen understanding of the phase memory time T_m, namely the timescale for the survival of quantum information stored in a freely-evolving spin qubit. While this process has yielded key design principles to lengthen T_m, one must not forget that spin qubits are partly envisaged for being employed in algorithms that will solve applied problems of wide interest and intractable by classical computers. Hence, the focus should eventually be put on the user-driven evolution of these qubits and on how they perform within the algorithm of interest subject to the mentioned relaxation mechanisms.

In this manuscript, we design a master equation aimed at time-evolving the density matrix of one spin qubit, where both the main relaxation rates and the user-driven control -in the form of pulse oscillating magnetic field- are inputted. This framework allows not only studying the mentioned problem that has drawn the attention over the last decade, namely to track the loss of quantum information as a magnetization decay in time when the spin freely evolves under relaxation without any external control, but also to tackle what the next step should be: the inclusion of the said external control to drive the spin in such a way that (i) free evolutions and rotations are combined as a gate sequence to place the qubit at those desired points of the Bloch sphere thus implementing any digital one-qubit algorithm while at the same time (ii) the main relaxation mechanisms extensively studied so far are active. Moreover, we also contribute with the detailed analytical resolution of the master equation. This facilitates an in-depth study of the qubit dynamics unlike when one follows the more extended procedure of employing numerical methods.

In the spirit of benchmarking the qubit performance within the desired algorithm as stated above, our work meets the long-term goal of developing certification protocols for quantum algorithms, where the fidelity between the density matrix obtained after running the algorithm and the expected one with neither relaxation nor experimental imperfections is the actual figure of merit instead of the timescale for the magnetization decay. The relaxation rates are rather an input of our master equation and hence this work connects in a natural way with all the theoretical efforts made over the past years devoted to compute them from *ab initio* methods. [47–62] In the race for the highly-prized scalable architectures, the realization of many-qubit systems will certainly depend on a proper understanding of the single-qubit dynamics under relaxation, external control, and imperfections as a key building block. Hence, we expect that our contribution will help to lay the foundations in the modeling of, firstly, qubit pairs for logical gates and, then, quantum algorithms involving larger numbers of qubits.

The master equation is handled via an open-source and user-friendly software package called QBithm, where the one-spin-qubit algorithms are established in the input as a gate sequence. We first demonstrate control over the whole Bloch sphere, and realize one-qubit gates whose fidelity is tested against relaxation and experimental imperfections. Then, we run well-known pulse sequences as instances of one-qubit algorithms, and obtain quantitative agreement with the experimental data of potential molecular spin qubits in the determination of the T_1, T_m and CPMG-sequence relaxation times as well as in the production of Rabi oscillations. Insight on the role of the vibration bath on spin qubit relaxation is also provided.

Results

Master equation

Our goal is to model the non-unitary time evolution of the spin qubit when its reduced density operator $\hat{\rho}(t \geq 0) = \mathrm{Tr}_{\mathrm{bath}}(\hat{\rho}_{\mathrm{qubit+bath}})$ is driven through a gate sequence under the influence of the most important relaxation sources affecting spin qubits, namely the vibration and spin baths. The spin qubit is pictured as an effective doublet whose states, termed as $|u_-\rangle$ and $|u_+\rangle$ with energies $u_- < u_+$, are selected from the energy scheme of the spin Hamiltonian $\hat{H}$ employed to describe the magnetic object containing the spin qubit. These states are not necessarily the ones with the lowest energies in the said scheme but should fulfil some specific requirements such as initialization and addressability in the form of an allowed and non-degenerate transition $|u_-\rangle \leftrightarrow |u_+\rangle$. We model such a time evolution by making use of the GKLS equation, also known as Lindblad master equation, which determines the effective dynamics within the subspace $\{|u_+\rangle, |u_-\rangle\}$ and, after adapta-

tion to our particular problem, reads as (see SI for a full description of all its elements):

$$\frac{\partial\hat{\rho}}{\partial t} \equiv \dot{\hat{\rho}} = \frac{1}{i\hbar}[\hat{H}_{\text{eff}}, \hat{\rho}] + \mathcal{L}_{\text{1-p}}\hat{\rho} + \mathcal{L}_{\text{2-p}}\hat{\rho} + \mathcal{L}_{\text{mag}}\hat{\rho} \quad (1)$$

In the characterization of the qubit-bath set, the use of the so-called Markovian approximation is legit since the timescale for the bath thermalization is much shorter than the one involved in the relaxation of the spin qubit. Correlations within the bath are lost extremely fast and this translates into a memoryless qubit+bath system such that its evolution is only determined by the current time step with no contribution from the past history. Any change induced by the qubit into the bath will rapidly be washed out and the bath itself recovers its thermal state quasi-instantaneously. This assures that no backflow of information from bath to qubit happens at any moment. The bath is thus statically described by its thermal density operator $\hat{\rho}^{\text{th}}_{\text{bath}} = \text{e}^{-\beta\hat{H}_{\text{bath}}}/\text{Z}$ only dependent on temperature.

Moreover, at the initial time $t = 0$, our gate sequences always start with the qubit placed in a given pure state $|\psi\rangle = \alpha\,|u_-\rangle + \beta\,|u_+\rangle$, $\alpha, \beta \in \mathbb{C}$, $|\alpha|^2 + |\beta|^2 = 1$, which is prepared apart from the bath. Hence, qubit and bath are supposed to be uncorrelated at $t = 0$ such that the global density operator $\hat{\rho}_{\text{qubit+bath}}(0)$ is expressed as the tensor product $\hat{\rho}(0) \otimes \hat{\rho}_{\text{bath}}(0)$ between qubit and bath degrees of freedom, being $\hat{\rho}(0) = |\psi\rangle\langle\psi|$. This assumption, known as Born approximation, combines with Markovianity in such a way that the above factorization extends over the whole time evolution with $\hat{\rho}_{\text{bath}}(t \geq 0) = \hat{\rho}^{\text{th}}_{\text{bath}}$ (weak qubit-bath coupling limit whereby the bath is not significantly altered due to its *largeness* compared to the qubit).

Last but not least, since the time of interest t for the propagation of $\hat{\rho}$ is in the μs scale or above -where the relaxation times of spin qubits lie- and the smallest timescale $T \lesssim 10^{-4}$ μs -given by typical spin qubit gaps $\gtrsim 10$ GHz- is much shorter than t, all fast oscillations associated to T are overshadowed and average out to zero in the timescale t of interest. This fact entitles one to disregard the said oscillations upon application of the so-called secular approximation, in virtue of which only the resonant interactions with the bath are retained. All in all, as soon as the above-mentioned approximations are justified in the characterization of the qubit-bath set, the non-unitary dynamics of the qubit induced by its coupling with the bath can be well described by the GKLS formalism. [63] The GKLS equation leads any initial state to a steady solution $\dot{\hat{\rho}}(t \to +\infty) = 0$ under free evolution (i.e. no user-induced driving), it is also Markovian, trace-preserving $\text{Tr}[\hat{\rho}(t \geq 0)] = 1$ and, unlike the Redfield master equation, is completely positive meaning that the non-negativity of the diagonal elements of $\hat{\rho}$ -the populations of the two qubit states- is guaranteed at any time.

The first term on the right-hand side of Eq.1 represents the unitary part of the qubit time evolution, while the remaining terms are the ones that induce the non-unitary dynamics on the qubit due to its interaction with the baths. In particular, $\mathcal{L}_{\text{1-p}}\hat{\rho}$ and $\mathcal{L}_{\text{2-p}}\hat{\rho}$ account for all the one- and two-phonon processes including both real (direct, Stokes/anti-Stokes, spontaneous emission followed by absorption) and virtual ones. These processes altogether are characterized by temperature-dependent absorption $\Gamma_{\text{ab}} \geq 0$ and emission $\Gamma_{\text{em}} \geq 0$ rates determining the flow of spin population between $|u_-\rangle$ and $|u_+\rangle$ driven by the vibration bath. [64] On the other hand, $\mathcal{L}_{\text{mag}}\hat{\rho}$ describes the effect of the spin bath on the qubit dynamics. [65] This bath is modeled as an isotropic magnetic noise -only dependent on the qubit-spin distances- and its effect is quantified by means of a rate $\Gamma_{\text{mag}} \geq 0$ whose magnitude is proportional to the volume concentration of spins in the bath. [49] All rates are time-independent and, crucially, non-negative which ensures the trace preservation and the complete positivity.

Given a time interval $t_{i-1} < t_i$ with $1 \leq i \leq n$ and $t_0 = 0$, t_n the initial and final evolution times, the effective Hamiltonian $\hat{H}_{\text{eff}}$ describes the spin qubit as a two-level system with an energy gap $u_+ - u_- = \hbar\omega_{+-}$ -being ω_{+-} the Larmor angular frequency- that is either freely evolved or driven in $t_{i-1} \leq t \leq t_i$ depending on whether the Rabi frequency $\Omega_{\text{R}} = \vec{\mu}_{+-} \cdot \vec{\mathbf{B}}_1/\hbar \in \mathbb{C}$ is zero or different from zero:

$$H_{\text{eff}} = \hbar \begin{pmatrix} \frac{\omega_{+-}}{2} & \Omega^*_{\text{R}}\cos(\omega_{\text{MW}}\Delta t^i) \\ \Omega_{\text{R}}\cos(\omega_{\text{MW}}\Delta t^i) & -\frac{\omega_{+-}}{2} \end{pmatrix} \quad (2)$$

All matrix representations are written in the ordered basis set $\{|u_+\rangle, |u_-\rangle\}$, $\Delta t^i = t - t_{i-1}$, $\vec{\mu}_{+-}$ is the magnetic dipolar moment associated to the transition $|u_-\rangle \leftrightarrow |u_+\rangle$, and $\vec{\mathbf{B}}_1$ is a linearly-polarized oscillating magnetic field whose angular frequency

is ω_{MW}. Essentially, if we neglect relaxation for a moment and $|\psi\rangle$ is parameterized in terms of the zenithal θ and azimuthal ϕ angles of the Bloch sphere, $|\psi\rangle = \cos(\theta/2)\,|u_-\rangle + \mathrm{e}^{i\phi}\mathrm{sen}(\theta/2)\,|u_+\rangle$ with $|0\rangle \equiv |u_-\rangle$ and $|1\rangle \equiv |u_+\rangle$, θ is controlled by activating $\vec{\mathbf{B}}_1$ for an appropriate time, while ϕ is changed by switching $\vec{\mathbf{B}}_1$ off and letting the Larmor precession make the qubit rotate around the axis joining the poles $|0\rangle$ and $|1\rangle$ of the said sphere with angular frequency ω_{+-} (see **Quantum gates for one-qubit algorithms** and SI).

Note that H_{eff} is time-dependent and this fact hampers the resolution of Eq.1 in the Schrödinger picture. It is thus crucial to devise a clever change of picture -namely a unitary operator $\hat{\mathcal{U}}$ transforming $\hat{\rho}$ into $\overline{\hat{\rho}} = \hat{\mathcal{U}}\hat{\rho}\hat{\mathcal{U}}^{\dagger}$- that allows eliminating the mentioned time-dependency to find the analytical solution of Eq.1. In our case, the right choice is:

$$\mathcal{U} = \begin{pmatrix} \exp\left(i\frac{\omega_{\mathrm{MW}}}{2}\Delta t^i\right) & 0 \\ 0 & \exp\left(-i\frac{\omega_{\mathrm{MW}}}{2}\Delta t^i\right) \end{pmatrix} \quad (3)$$

All details concerning the analytical resolution of Eq.1 in the above picture are found in SI. In this resolution, we make use of the rotating wave approximation and the resulting effective Hamiltonian $\overline{H}_{\mathrm{eff}}$ in the new picture -with no time-dependency but dependent on the detuning $\delta = \omega_{+-} - \omega_{\mathrm{MW}}$- is:

$$\overline{H}_{\mathrm{eff}} = \frac{\hbar}{2}\begin{pmatrix} \delta & \Omega_{\mathrm{R}}^* \\ \Omega_{\mathrm{R}} & -\delta \end{pmatrix} \quad (4)$$

A given initial condition at $t = t_0$ for the density operator $\overline{\hat{\rho}}$ provides a unique solution of Eq.1. Note that $\hat{\mathcal{U}}(t = t_0) = \hat{I}$ -the identity operator- meaning that at $t = t_0$ Schrödinger and new pictures coincide. Hence, the said initial condition can be given on the density operator $\hat{\rho}$. If we consider the matrix representation $\rho(t = t_0) = \rho_{11}^0\,|u_+\rangle\langle u_+| + (\rho_{12,r}^0 + i\rho_{12,i}^0)\,|u_+\rangle\langle u_-| + (\rho_{12,r}^0 - i\rho_{12,i}^0)\,|u_-\rangle\langle u_+| + \rho_{22}^0\,|u_-\rangle\langle u_-|$, one just needs to provide the four real numbers ρ_{11}^0, ρ_{22}^0, $\rho_{12,r}^0$, $\rho_{12,i}^0$ with $\rho_{11}^0 + \rho_{22}^0 = 1$. As mentioned above, the case of interest for us is to prepare the qubit in a pure state $|\psi\rangle = \alpha\,|u_-\rangle + \beta\,|u_+\rangle$ at $t = t_0$, with $\alpha = \alpha_r + i\alpha_i$, $\beta = \beta_r + i\beta_i$, $|\alpha|^2 + |\beta|^2 = 1$. By working out $|\psi\rangle\langle\psi|$, one easily finds $\rho_{11}^0 = |\beta|^2, \rho_{22}^0 = |\alpha|^2, \rho_{12,r}^0 = \beta_r\alpha_r + \beta_i\alpha_i, \rho_{12,i}^0 = \beta_i\alpha_r - \beta_r\alpha_i$. In the production of Rabi oscillations and determination of T_1, T_m, we use $\alpha = 1$, $\beta = 0$ (see **Pulse sequences: Rabi oscillations and spin relaxation times**).

Once Eq.1 is transformed into the new picture, let us note that its solutions can be classified in two main groups depending on whether $\Gamma_{\mathrm{ab}} = \Gamma_{\mathrm{em}} = \Gamma_{\mathrm{mag}} = 0$ or at least one of these rates is different from zero. In the first case, where no relaxation takes place and the qubit behaves as a closed system with a unitary dynamics, the Liouville-von Neumann equation $i\hbar\dot{\overline{\rho}} = [\overline{H}_{\mathrm{eff}}, \overline{\rho}]$ is recovered. Its solution -fully described in SI- is given by $\overline{\rho}(t_{i-1} \leq t \leq t_i) = \mathcal{R}\rho(t_{i-1})\mathcal{R}^{\dagger}$ being $\mathcal{R} = \exp\left(-i\Delta t^i\overline{H}_{\mathrm{eff}}/\hbar\right)$ the rotation operator, or $\overline{|\psi\rangle}(t_{i-1} \leq t \leq t_i) = \mathcal{R}\,|\psi\rangle$ in case of pure states. The computation of $\mathcal{R}$ shows that it depends on the so-called generalized Rabi frequency $\Omega_{\mathrm{g}} = \sqrt{|\Omega_{\mathrm{R}}|^2 + \delta^2}$ and that a rotation angle can be defined as $\Omega_{\mathrm{g}}\Delta t_i$ with $\Delta t_i = t_i - t_{i-1}$ interpreted as the time taken by the rotation.

When $\delta = 0$, the representation of $\mathcal{R}$ is that of a 2D rotation matrix and, if the qubit is described by a pure state $|\psi\rangle = \cos(\theta/2)\,|u_-\rangle + \mathrm{e}^{i\phi}\mathrm{sen}(\theta/2)\,|u_+\rangle$, $\mathcal{R}$ rotates $|\psi\rangle$ an angle $\Omega_{\mathrm{g}}\Delta t_i$ around the axis perpendicular to the plane containing $|\psi\rangle$, $\mathcal{R}\,|\psi\rangle$, and the origin $\mathcal{O}$ of the Bloch sphere. Since $\mathcal{R}$ is unitary, the norm of $|\psi\rangle$ is conserved and $\mathcal{R}\,|\psi\rangle$ is also found on the mentioned sphere. In case the rotation axis is contained in the equatorial plane of the Bloch sphere, and for that to happen the plane defined by $\{|\psi\rangle, \mathcal{R}\,|\psi\rangle, \mathcal{O}\}$ must contain the line joining the poles $|0\rangle$ and $|1\rangle$, one finds that $\mathcal{R}\,|\psi\rangle = \cos((\theta+\Omega_{\mathrm{g}}\Delta t_i)/2)\,|u_-\rangle + \mathrm{e}^{i\phi}\mathrm{sen}((\theta+\Omega_{\mathrm{g}}\Delta t_i)/2)\,|u_+\rangle$. Namely, the rotation has been performed along the meridian given by the unaltered azimuthal angle ϕ and the rotation angle $\theta + \Omega_{\mathrm{g}}\Delta t_i - \theta = \Omega_{\mathrm{g}}\Delta t_i$ can be interpreted here as a zenithal angle.

When $|\psi\rangle = |u_-\rangle$, namely $\theta = 0$, this case often defines the starting point of EPR-pulse experiments in which the qubit is initialized in its lowest energy state. If Δt_i is such that $\Omega_{\mathrm{g}}\Delta t_i = \pi/2$ or $\Omega_{\mathrm{g}}\Delta t_i = \pi$, $\mathcal{R}$ corresponds to the well-known $\pi/2$ and π pulses: the first one creates an equally-weighted superposition $|\mathrm{ew}\rangle$ between $|u_-\rangle$ and $|u_+\rangle$ contained in the equatorial plane of the Bloch sphere, while the second one transfers all the spin population from $|0\rangle \equiv |u_-\rangle$ to $|1\rangle \equiv |u_+\rangle$. Instead, if $\delta \neq 0$, $\mathcal{R}(\Omega_{\mathrm{g}}\Delta t_i = \pi/2)\,|u_-\rangle$ and $\mathcal{R}(\Omega_{\mathrm{g}}\Delta t_i = \pi)\,|u_-\rangle$ will differ from $|\mathrm{ew}\rangle$ and $|u_+\rangle$, resp. The realization of a rotation in such a way that the resulting state lies close enough to the expected one crucially depends

on how small δ is (see **Quantum gates for one-qubit algorithms**) and hence δ should be taken as a key design parameter.

In the other main group of solutions of Eq.1 transformed into the new picture, at least one of the three rates $\Gamma_{\rm ab}$, $\Gamma_{\rm em}$, $\Gamma_{\rm mag}$ is different from zero. In this situation, there exists in turn two subgroups of solutions depending on whether both $|\vec{\mathbf{B}}_1|$ and $\omega_{\rm MW}$ are zero, or $|\vec{\mathbf{B}}_1| \neq 0$ and $\omega_{\rm MW} \neq 0$. These subgroups constitute the two elementary building-blocks that we will employ sequentially in the form of gates for the construction of one-qubit algorithms. The first gate -detailed in SI- is known as free evolution: the qubit evolves for a given time subject to relaxation but with no user-induced driving. For instance, this evolution can be encountered (i) during the waiting time between pulses such as the $\pi/2$ and π pulses of the Hahn sequence and (ii) after the said π pulse of the same sequence until recording the Hahn echo.

On the other hand, the gate consisting in $|\vec{\mathbf{B}}_1| \neq 0$ and $\omega_{\rm MW} \neq 0$ also for a finite time Δt_i is known as rotation: the qubit is now driven by the user but, since relaxation is active, its evolution cannot be described in terms of a pure state circulating on the Bloch sphere anymore. Notwithstanding, when Δt_i is short enough as compared to the relaxation timescale t_r set by $\Gamma_{\rm ab}$, $\Gamma_{\rm em}$, $\Gamma_{\rm mag}$, the qubit evolves quasi-unitarily and the Bloch sphere picture can still be recovered. For instance, this situation applies in the description of the $\pi/2$ and π pulses which take a few tens of nanoseconds in standard EPR experiments, while typical relaxation times in spin qubits lie in the microsecond scale or above (see **Quantum gates for one-qubit algorithms**). Under this circumstance, the solution $\overline{\rho}(t = t_i)$ provided by our master equation Eq.1 in the new picture can be approximated by the one obtained above with the rotation operator $\mathcal{R}$ at $t = t_i$. If additionally $\delta \to 0$, $\mathcal{R}$ is often directly expressed in terms of the rotation angle ζ, namely $\mathcal{R}(\zeta)$, with no presence of $\Omega_{\rm g}$ and Δt_i thus assuming that both $\Omega_{\rm g}$ and Δt_i are properly chosen in the lab such that their combination produces the desired value of ζ. [50]

Our solution $\overline{\rho}(t = t_i)$ mentioned above generalizes the one produced by $\mathcal{R}(\zeta)$ and provides a more realistic description of rotations since the former (i) always contains the effects of relaxation -whether they are small or large after Δt_i-, (ii) can deal with values $\delta \neq 0$, and (iii) provides the user with full control by inputting $|\vec{\mathbf{B}}_1|$, $\omega_{\rm MW}$ -both determining δ and $\Omega_{\rm g}$-, and Δt_i, instead of directly using ζ. Moreover, whether δ is small or large, relaxation becomes significant when $\Delta t_i \gtrsim t_r$, a fact that precludes the use of $\mathcal{R}$ at $t = t_i$ and obliges to employ $\overline{\rho}(t = t_i)$. This is the case of the production of Rabi oscillations where the rotation -named as nutation- is extended with a duration that ranges from $\Delta t_1 \sim t_0$ to $\Delta t_1 \sim t_r$. While $\overline{\rho}(t_0 \leq t \leq t_1)$ is able to reproduce the damping of these oscillations caused by relaxation as t moves on (see **Pulse sequences: Rabi oscillations and spin relaxation times**), $\mathcal{R}$ would just produce non-damped oscillations.

With these ingredients and given $\rho(t = t_0)$, any digital one-qubit algorithm is simply constructed as a finite sequence $\{G_i\}_{i=1}^{n}$ of free evolutions and rotations: $\rho(t = t_0) \xrightarrow{G_1,\Delta t_1} \cdots \xrightarrow{G_{i-1},\Delta t_{i-1}} \overline{\rho}(t_{i-1}) \xrightarrow{G_i,\Delta t_i} \overline{\rho}(t_i) \xrightarrow{G_{i+1},\Delta t_{i+1}} \cdots \xrightarrow{G_n,\Delta t_n} \overline{\rho}(t_n)$, where each G_i is activated for a time $\Delta t_i = t_i - t_{i-1}$ and transforms $\overline{\rho}(t_{i-1})$ as an initial condition into $\overline{\rho}(t_i)$ via Eq.1 -in the new picture- with $t_0 = 0$ and $\overline{\rho}(t_0) = \rho(t = t_0)$. In case of not being interested in any observable, one can either (i) just follow the evolution of $\overline{\rho}$ after each G_i or (ii) even repeat the same algorithm but with $\Gamma_{\rm ab} = \Gamma_{\rm em} = \Gamma_{\rm mag} = 0$ in order to obtain a new result $\overline{\rho}^0(t_n)$ and calculate the fidelity between $\overline{\rho}(t_n)$ and $\overline{\rho}^0(t_n)$ as a performance measure of the qubit in the algorithm (see **Quantum gates for one-qubit algorithms**).

Now, given an observable O in the Schrödinger picture and represented in the ordered basis set $\{|u_+\rangle, |u_-\rangle\}$, its expectation value $\langle O\rangle(t_n)$ at $t = t_n$ can be determined as $\langle O\rangle(t_n) = {\rm Tr}[O\rho(t_n)]$ where $\rho(t_n) = \mathcal{U}^\dagger(\Delta t_n)\overline{\rho}(t_n)\mathcal{U}(\Delta t_n)$. Two observables of interest are the longitudinal ${\rm M}_z = \sigma_z = |u_+\rangle\langle u_+| - |u_-\rangle\langle u_-|$ and in-plane ${\rm M}_{xy} = \sigma_x + i\sigma_y = 2|u_+\rangle\langle u_-|$ magnetizations as they are employed in the determination of Rabi oscillations and T_1, T_m (see **Pulse sequences: Rabi oscillations and spin relaxation times**). If $\overline{\rho}(t_n) = \overline{\rho}_{11}(t_n)|u_+\rangle\langle u_+| + (\overline{\rho}_{12,r}(t_n) + i\overline{\rho}_{12,i}(t_n))|u_+\rangle\langle u_-| + (\overline{\rho}_{12,r}(t_n) - i\overline{\rho}_{12,i}(t_n))|u_-\rangle\langle u_+| + \overline{\rho}_{22}(t_n)|u_-\rangle\langle u_-|$, we find in SI: $\langle {\rm M}_z\rangle(t_n) = \overline{\rho}_{11}(t_n) - \overline{\rho}_{22}(t_n)$ and $\langle {\rm M}_{xy}\rangle(t_n) = 2\left(\overline{\rho}_{12,r}(t_n)\cos(\Delta t_n\omega_{\rm MW}) + \overline{\rho}_{12,i}(t_n)\,{\rm sen}(\Delta t_n\omega_{\rm MW})\right) + i2\left(\overline{\rho}_{12,r}(t_n)\,{\rm sen}(\Delta t_n\omega_{\rm MW}) - \overline{\rho}_{12,i}(t_n)\cos(\Delta t_n\omega_{\rm MW})\right)$. Note that $\langle {\rm M}_{xy}\rangle(t_n)$ -with oscillatory real and imaginary parts- is complex. In order to compare with experimental data, we use the absolute value

$|\langle \mathrm{M}_{xy}\rangle(t_n)| = 2\sqrt{(\overline{\rho}_{12,r}(t_n))^2 + (\overline{\rho}_{12,i}(t_n))^2}$.

Whenever G_i consists in a free evolution, it is possible to analytically find $\overline{\rho}(t_i)$ as an explicit function of $\overline{\rho}(t_{i-1})$. In particular, if $G_{i=n}$ is a free evolution, the further work out of $\langle \mathrm{M}_z\rangle(t_n)$ and $|\langle \mathrm{M}_{xy}\rangle(t_n)|$ provides the explicit relation between Γ_{ab}, Γ_{em}, Γ_{mag} and the decay rates Γ_1, Γ_2 of $\langle \mathrm{M}_z\rangle(t_n)$ and $|\langle \mathrm{M}_{xy}\rangle(t_n)|$ plotted vs Δt_n (see SI). This is of specific interest since the last gate in the pulse sequences employed to experimentally determine the respective decay timescales T_1 and T_m of $\langle \mathrm{M}_z\rangle$ and $|\langle \mathrm{M}_{xy}\rangle|$ consists in a free evolution with a variable duration time (see **Pulse sequences: Rabi oscillations and spin relaxation times**). We find that $\langle \mathrm{M}_z\rangle(t_n)$ decays single-exponentially in Δt_n with a rate $\Gamma_1 = \Gamma_{\mathrm{ab}} + \Gamma_{\mathrm{em}} + \Gamma_{\mathrm{mag}}$, while the decay of the real and imaginary parts of $\langle \mathrm{M}_{xy}\rangle(t_n)$ in Δt_n is double-exponentially with rates Γ_1 and $\Gamma_2 = (\Gamma_{\mathrm{ab}} + \Gamma_{\mathrm{em}})/2 + \Gamma_{\mathrm{mag}}$.

The said exponential decays with Δt_n are non-stretched and this fact may hamper a proper description by our theoretical model of those experiments where the processes that produce an stretched shape of the magnetization are the ones that determine the observed spin relaxation. [48] We also find that the decay of the real and imaginary part of $\langle \mathrm{M}_{xy}\rangle(t_n)$ is oscillatory with angular frequency ω_{+-}. Hence, oscillations in $|\langle \mathrm{M}_{xy}\rangle|(t_n)$ with Δt_n could appear. When the spin that encodes the qubit is coupled with a neighboring nuclear spin, e.g. that of ^{1}H, the experimental $|\langle \mathrm{M}_{xy}\rangle|$ could also exhibit an oscillatory decay but now with the nuclear Larmor frequency of ^{1}H. This situation whereby the Larmor frequency of an external spin coupled to the spin qubit determines the oscillation frequency of the mentioned magnetization decay is also beyond the reach of our model. A proper description of this phenomenon would require to expand the qubit 2D Hilbert space to include the coupled nuclear spin in the qubit dynamics.

Case studies

The *ab initio* calculation of $\vec{\mu}_{+-}$, Γ_{ab}, Γ_{em}, Γ_{mag} requires using the energy scheme -including $|u_-\rangle$, $|u_+\rangle$, u_-, u_+- of the spin Hamiltonian $\hat{H}$ that models the magnetic object containing the spin qubit. The particular scheme we focus on is that described by a ground electron spin quantum number $S \geq 1/2$ either effective or not. An instance of an effective S can be encountered when a set of angular momenta S_i couple with each other at low enough temperature thus producing a giant ground spin S. In case of non-negligible spin-orbit interactions with an orbital quantum number $L \neq 0$, S would be replaced by the total electron spin J as a good quantum number. Henceforth, we use J where the particular case $L = 0$, $J = S$ is included. We also neglect interactions between J and higher energy states arising from excited quantum numbers J_{ex}. This means that any working temperature should be low enough as compared to the gap between the J manifold comprising $2J+1$ states and that of the first excited J_{ex}.

The quantum number J -associated to a ground electron spin operator $\hat{\vec{\mathbf{J}}} = (\hat{J}_x, \hat{J}_y, \hat{J}_z)$ with Cartesian components $\{\hat{J}_\alpha\}_{\alpha=x,y,z}$- is combined with up to three types of interactions. First, with an external, weak, and static magnetic field $\vec{\mathbf{B}} = (B_x, B_y, B_z)$. This interaction is described in terms of a Zeeman Hamiltonian. Second, an important class of magnetic objects of interest for us is that of molecular coordination complexes, where one or several magnetic atoms or magnetic atomic ions are surrounded by and linked to a set of donor atoms via coordinate covalent bonds. The electrostatic field produced by the donor atoms lifts the initial degeneracy of the $2J+1$ states thus producing a zero-field splitting. This fact is accounted for with the inclusion of the so-called Crystal Field Hamiltonian, which is also employed in the description of another relevant class of magnetic objects as that of nitrogen-vacancy centers in nanodiamonds. Third, in case of having a ground nuclear spin quantum number I, the J-manifold can be further expanded by coupling J to I with a hyperfine interaction term. All in all, the spin Hamiltonian $\hat{H}$ whose energy scheme (i) $|u_-\rangle$, $|u_+\rangle$, u_-, u_+ are selected from, and (ii) we employ to calculate $\vec{\mu}_{+-}$, Γ_{ab}, Γ_{em}, Γ_{mag} (see SI and [47, 49] for details), reads as follows:

$$\hat{H} = \frac{\mu_B}{\hbar} \sum_{\alpha=x,y,z} g_\alpha B_\alpha \hat{J}_\alpha + \sum_{k,q} B_k^q \hat{O}_k^q + \qquad (5)$$

$$+ \sum_{\beta=x,y,z} A_\beta \hat{I}_\beta \hat{J}_\beta + P\hat{I}_z^2$$

The first term in Eq.5 is the Zeeman Hamiltonian, being μ_B the Bohr magneton, $\hbar$ the reduced

Planck's constant, and g_α the effective Landé factors. The reason for allowing g_α be different among them and different from g_J -the free J Landé factor- is to effectively recover the electron spin anisotropy -either small or large- in case ones sets $B_k^q \equiv 0$ not to employ the Crystal Field Hamiltonian. When employing it, we set $g_\alpha = g_J$. The second term is the said Crystal Field Hamiltonian which is written as a function of the Crystal Field Parameters B_k^q and the Extended Stevens Operators $\hat{O}_k^q$ with $k = 2, 4, 6$ and $q = -k, -k+1, ..., k-1, k$. The third term describes the hyperfine interaction between $\hat{\vec{\mathbf{J}}}$ and the ground nuclear spin operator $\hat{\vec{\mathbf{I}}} = (\hat{I}_x, \hat{I}_y, \hat{I}_z)$ associated to I with parameters $\{A_\beta\}_{\beta=x,y,z}$, while the fourth one models a possible zero-field splitting of I with parameter P.

The above spin Hamiltonian encompasses a large set of wide-interest systems employed to define spin qubits in the energy scheme described by Eq.5. Well-known instances are quantum dots in heterostructures such as GaAs, vacancy centers in SiC and nanodiamonds, group VA dopant atoms in silicon, transition metal and rare-earth impurities in ionic crystals, and molecular coordination complexes with a single magnetic atomic ion such as V^{4+}, Cu^{2+} or Ln^{3+} where Ln = Gd, Tb, Dy, Ho. The two states $|u_-\rangle$ and $|u_+\rangle$ of the spin qubit are selected among the $(2J+1)(2I+1)$ states obtained after diagonalizing Eq.5.

As previously seen, when the last gate of the sequence is a free evolution, we find analytical expressions for $\langle \mathrm{M}_z\rangle(t_n)$ and $|\langle \mathrm{M}_{xy}\rangle(t_n)|$ as explicit functions of Γ_{ab}, Γ_{em}, Γ_{mag}. Importantly, the decay of $\langle \mathrm{M}_z\rangle(t_n)$ and $|\langle \mathrm{M}_{xy}\rangle(t_n)|$ with Δt_n -as determined by the said three rates- is exponential but non-stretched. In order to incorporate other possible spin relaxation processes which also produce a non-stretched exponential decay of $\langle \mathrm{M}_z\rangle(t_n)$ and $|\langle \mathrm{M}_{xy}\rangle(t_n)|$ but that are not included in Γ_{ab}, Γ_{em}, Γ_{mag}, we add $\Gamma_{\mathrm{ab,add}} \geq 0$, $\Gamma_{\mathrm{em,add}} \geq 0$, $\Gamma_{\mathrm{mag,add}} \geq 0$ up to Γ_{ab}, Γ_{em}, Γ_{mag} such that $\Gamma_{\mathrm{a}} := \Gamma_{\mathrm{ab}} + \Gamma_{\mathrm{ab,add}}$, $\Gamma_{\mathrm{e}} := \Gamma_{\mathrm{em}} + \Gamma_{\mathrm{em,add}}$, $\Gamma_{\mathrm{m}} := \Gamma_{\mathrm{mag}} + \Gamma_{\mathrm{mag,add}}$ are the actual rates employed in Eq.1 with $\Gamma_{\mathrm{ab,add}}$, $\Gamma_{\mathrm{em,add}}$, $\Gamma_{\mathrm{mag,add}}$ to be used as free parameters when not set to zero. Optionally, this set of added rates can be reduced into two parameters by relating $\Gamma_{\mathrm{ab,add}}$ and $\Gamma_{\mathrm{em,add}}$ through the detailed balance condition at a given temperature T:

$$\Gamma_{\mathrm{ab,add}} = \Gamma_{\mathrm{em,add}} \exp\left(-(u_+ - u_-)/k_{\mathrm{B}}T\right) \qquad (6)$$

The rates $\Gamma_{\mathrm{ab,add}}$, $\Gamma_{\mathrm{em,add}}$, $\Gamma_{\mathrm{mag,add}}$ may still have an alternative role to that just described. Indeed, in case a rather different spin Hamiltonian is preferred over Eq.5, one would set $\Gamma_{\mathrm{ab}} = \Gamma_{\mathrm{em}} = \Gamma_{\mathrm{mag}} = 0$ and input in $\vec{\mu}_{+-}$, $\Gamma_{\mathrm{ab,add}}$, $\Gamma_{\mathrm{em,add}}$, $\Gamma_{\mathrm{mag,add}}$ the values of the magnetic dipolar moment, absorption, emission, and magnetic rates calculated with the energy scheme, which $\{|u_-\rangle, |u_+\rangle, u_-, u_+\}$ are now taken from, of the desired spin Hamiltonian. An instance of the latter could be the expansion of Eq.5 with the excited quantum numbers J_{ex}.

QBithm software package

All in all, the input required to implement a given digital quantum algorithm involving a single spin qubit consists of (i) the initial condition $\rho(t = t_0)$ provided by the four real numbers ρ_{11}^0, ρ_{22}^0, $\rho_{12,r}^0$, $\rho_{12,i}^0$ with $\rho_{11}^0 + \rho_{22}^0 = 1$, and (ii) the finite sequence $\{G_i\}_{i=1}^n$ where each G_i is the time propagation of $\overline{\rho}$ from $\overline{\rho}(t_{i-1})$ to $\overline{\rho}(t_i)$ via Eq.1 with $t_0 = 0$ and $\overline{\rho}(t_0) = \rho(t = t_0)$. Each G_i is selected with either $|\vec{\mathbf{B}}_1| = 0$ and $\omega_{\mathrm{MW}} = 0$ -case of a free evolution- or $|\vec{\mathbf{B}}_1| \neq 0$ and $\omega_{\mathrm{MW}} \neq 0$ -case of a rotation-. The output of interest can be found either at checking each $\overline{\rho}(t_i)$ to follow the time evolution of the qubit and using $\overline{\rho}(t_n)$ to compute the resulting fidelity by repeating the algorithm with $\Gamma_{\mathrm{a}} = \Gamma_{\mathrm{e}} = \Gamma_{\mathrm{m}} = 0$, or at calculating both $\langle \mathrm{M}_z\rangle(t_n)$ and $|\langle \mathrm{M}_{xy}\rangle(t_n)|$ as a function of t_n when this time is variable.

In this last case, $\langle \mathrm{M}_z\rangle(t_n)$ and $|\langle \mathrm{M}_{xy}\rangle(t_n)|$ are plotted vs Δt_{i_0}, for some $1 \leq i_0 \leq n$, inside a selected range from $\Delta t_{i_0} \gtrsim 0$ until $\langle \mathrm{M}_z\rangle(t_n)$ and $|\langle \mathrm{M}_{xy}\rangle(t_n)|$ vanish. In some sequences, apart from Δt_{i_0}, other time intervals Δt_i are also simultaneously varied within the same range. Being $1 \leq m \leq n$ the number of these variable time intervals which we rename as $\tau := \Delta t_i$ including $i = i_0$, the plot of $\langle \mathrm{M}_z\rangle(t_n)$ and $|\langle \mathrm{M}_{xy}\rangle(t_n)|$ is performed vs $m\tau$.

For instance, the Hahn sequence, with $\rho_{22}^0 = 1$, $\rho_{11}^0 = \rho_{12,r}^0 = \rho_{12,i}^0 = 0$, $m = 2$, consists of $n = 4$ gates where G_1 is a $\pi/2$ rotation, G_3 is a π rotation, and G_2, G_4 are a free evolution with the same variable duration time -known as waiting time- τ. The plot of interest is that of representing $|\langle \mathrm{M}_{xy}\rangle(t_4)|$ vs 2τ, and the use of a fitting curve f -often of the form

$f(2\tau) = a + b\exp(-2\tau/T_m)$- allows determining the theoretical value of T_m. On the other hand, the so-called Inversion Recovery sequence, with the same initial condition, consists of $n = 2$ gates being G_1 a π rotation and G_2 a free evolution with a variable τ. In this case, $m = 1$ and the theoretical value of T_1 is obtained after fitting the plot $\langle \mathrm{M}_z\rangle(t_2)$ vs τ often to the curve $f(\tau) = a(1 - b\exp(-\tau/T_1))$. Since the T_1 to obtain remains the same, we have rather coded in QBithm: $\langle \mathrm{M}_z\rangle(t_n) = \overline{\rho}_{22}(t_n) - \overline{\rho}_{11}(t_n)$. Last, the sequence to produce Rabi oscillations, where $\rho^0_{22} = 1$, $\rho^0_{11} = \rho^0_{12,r} = \rho^0_{12,i} = 0$ again, consists of a single $n = 1$ gate, namely a rotation but now with a variable τ. The plot to perform is $\langle \mathrm{M}_z\rangle(t_1)$ vs τ.

In the experimental determination of Rabi oscillations and T_1, the sequences presented above are still further extended with an extra set of pulses which are necessary to measure the relevant magnetization. From theory, we can compute the magnetization at any moment hence there is no need to incorporate the said extra pulses. Yet, we use one of the case studies below to check in SI that no significant difference in the results is found when the original sequences are extended.

We have coded the above-summarized procedures in the form of an open-source and user-friendly Fortran 77 software package named as QBithm, whose detailed user handbook can be found in SI. The code is fed via three input files: qb.ddata, qb.mdata, and qb.adata. The first one contains, for each field direction $\vec{\mathbf{B}}/|\vec{\mathbf{B}}|$ to explore: Γ_{mag}, the $(2J+1)(2I+1)$ spin energies E_i of Eq.5, as well as the matrix elements N_{+-} and M_{+-} -computed from the states of Eq.5- necessary to calculate $\vec{\mu}_{+-}$ and Γ_{ab}, Γ_{em}, resp. On its hand, qb.mdata includes the harmonic frequency, reduced mass, and half-width of each mode in the vibration bath. The automated generation of qb.ddata, qb.mdata and the computation of all parameters therein is accomplished by employing the code SIMPRE, [47] which operates under Eq.5 and can be obtained from the authors upon request. It is also possible to sweep $|\vec{\mathbf{B}}|$ in qb.ddata in order to produce ESE(electron spin echo)-detected spectra. For this purpose, one employs the Hahn sequence with a fixed τ, and then plots $|\langle \mathrm{M}_{xy}\rangle(t_4)|$ vs $|\vec{\mathbf{B}}|$. The third input file, qb.adata, is the place where the gates $\{G_i\}_{i=1}^n$ are established thus setting up the desired one-spin-qubit algorithm or pulse sequence. It also contains the duration time Δt_i of the implemented free evolutions and rotations along with the axes of the latter. Extra input parameters that may also need to be set such as the numerical value of $(2J + 1)(2I + 1)$, the temperature T, g_J, $|\vec{\mathbf{B}}_1|$, $\omega_{\mathrm{MW}}/2\pi$, $\Gamma_{\mathrm{ab,add}}$, $\Gamma_{\mathrm{em,add}}$, $\Gamma_{\mathrm{mag,add}}$, ρ^0_{11}, ρ^0_{22}, $\rho^0_{12,r}$, $\rho^0_{12,i}$ are found in the code file qbithm.f.

On the other hand, up to three output files can be generated: (i) qb.out, where one can read δ, Ω_{g}, Γ_{ab}, Γ_{em}, the vibration modes in qb.mdata that most contribute to these two rates, and $\overline{\rho}(t_i)$ at each t_i, (ii) qb.mz.out, with $\langle \mathrm{M}_z\rangle(t_n)$ vs $m\tau$, and (iii) qb.mxy.out, containing $|\langle \mathrm{M}_{xy}\rangle(t_n)|$ vs $m\tau$. When $m = 0$, qb.mz.out and qb.mxy.out just contain a single value of $\langle \mathrm{M}_z\rangle(t_n)$ and $|\langle \mathrm{M}_{xy}\rangle(t_n)|$, namely the values corresponding to the set of fixed time intervals $\{\Delta t_i\}_{i=1}^n$. Both plotting and curve fitting is not performed by QBithm and one must use a rather different code devoted to these tasks.

Let us stress that SIMPRE can be requested to write in qb.ddata either $\Gamma_{\mathrm{mag}} = 0$ or its *ab initio* value after determining it. On the other hand, QBithm computes Γ_{ab} and Γ_{em} from qb.ddata and qb.mdata as generated by SIMPRE. Instead, if $\Gamma_{\mathrm{ab}} = \Gamma_{\mathrm{em}} = 0$ is desired, the user requests SIMPRE not to generate qb.mdata nor to write M_{+-} in qb.ddata thus leading QBithm to automatically implement the above setting. The option $\Gamma_{\mathrm{ab}} = \Gamma_{\mathrm{em}} = 0$ applies in the following cases: (i) if using Eq.5, to employ qb.ddata as produced by SIMPRE with Γ_{mag} either zero or its *ab initio* value, while each $\Gamma_{\mathrm{ab,add}}$, $\Gamma_{\mathrm{em,add}}$, $\Gamma_{\mathrm{mag,add}}$ is either zero or operated as a free parameter, (ii) if using a spin Hamiltonian $\hat{H}$ different from Eq.5, each $\Gamma_{\mathrm{ab,add}}$, $\Gamma_{\mathrm{em,add}}$, $\Gamma_{\mathrm{mag,add}}$ can be zero, *ab initio*, or free parameter; in addition, SIMPRE can still be requested to generate qb.ddata with $\Gamma_{\mathrm{mag}} = 0$ but, prior to run QBithm and for each field direction $\vec{\mathbf{B}}/|\vec{\mathbf{B}}|$, one will first manually replace (a) all E_i by only u_-, u_+ -thus using $(2J + 1)(2I + 1) = 2$ in qbithm.f- calculated from the said $\hat{H}$, and (b) the values of N_{+-} by the ones also calculated with $\hat{H}$. Recall that, whenever one desires using Eq.6, $\Gamma_{\mathrm{ab,add}}$ is not inputted but automatically computed by QBithm from the given $\Gamma_{\mathrm{em,add}}$ value whether this is *ab initio* or free parameter, with $\Gamma_{\mathrm{em,add}} = 0$ producing $\Gamma_{\mathrm{ab,add}} = 0$.

All in all, QBithm can be operated in three ways: (i) *ab initio* mode, where one either sets $\Gamma_{\mathrm{ab,add}} = \Gamma_{\mathrm{em,add}} = \Gamma_{\mathrm{mag,add}} = 0$ and uses qb.ddata, qb.mdata as produced by SIMPRE with Eq.5, or

sets $\Gamma_{\rm ab} = \Gamma_{\rm em} = \Gamma_{\rm mag} = 0$ and -as above explained- inputs $(2J+1)(2I+1) = 2$, u_-, u_+, N_{+-}, $\Gamma_{\rm ab,add}$, $\Gamma_{\rm em,add}$, $\Gamma_{\rm mag,add}$ computed by the user with the desired $\hat{H}$, (ii) semi-empirical mode, where $\Gamma_{\rm ab} = \Gamma_{\rm em} = \Gamma_{\rm mag} = 0$ and $\Gamma_{\rm ab,add}$, $\Gamma_{\rm em,add}$, $\Gamma_{\rm mag,add}$ are employed to fit experimental data, (iii) any meaningful combination of (i) and (ii), where, if at least one set among $\{\Gamma_{\rm ab}, \Gamma_{\rm em}\}$, $\{\Gamma_{\rm mag}\}$ is *ab initio*, all rates $\Gamma_{\rm ab,add}$, $\Gamma_{\rm em,add}$, $\Gamma_{\rm mag,add}$ must be either zero or free parameter, and vice versa: if any rate among $\Gamma_{\rm ab,add}$, $\Gamma_{\rm em,add}$, $\Gamma_{\rm mag,add}$ is *ab initio*, both $\{\Gamma_{\rm ab}, \Gamma_{\rm em}\}$ and $\{\Gamma_{\rm mag}\}$ must be either zero or free parameter. The reason is to avoid the joint use of rates determined with different spin Hamiltonians as N_{+-}, M_{+-}, E_i would remain undefined.

We have not coded $\mathcal{R}$ in QBithm. Despite it, the main group of solutions $\Gamma_{\rm a} = \Gamma_{\rm e} = \Gamma_{\rm m} = 0$ -namely $\Gamma_{\rm ab} = \Gamma_{\rm em} = \Gamma_{\rm mag} = \Gamma_{\rm ab,add} = \Gamma_{\rm em,add} = \Gamma_{\rm mag,add} = 0$- can be easily recovered. For mathematical reasons (see SI), one must avoid setting $\Gamma_{\rm ab} = \Gamma_{\rm em} = \Gamma_{\rm mag} = \Gamma_{\rm ab,add} = \Gamma_{\rm em,add} = \Gamma_{\rm mag,add} = 0$. Instead, all six rates are set to zero but one -usually $\Gamma_{\rm mag,add}$- which is given a value close to zero yet above the machine precision (e.g. $10^{-10} - 10^{-12}$ μs^{-1}, such that $10^{10} - 10^{12}$ μs is much larger than any runtime meaning relaxation is effectively neglected).

Quantum gates for one-qubit algorithms

Rotation and free evolution can be combined in QBithm to place the spin qubit at any point of the Bloch sphere. If $|\psi\rangle = \cos(\theta/2)\,|0\rangle + {\rm e}^{i\phi}{\rm sen}(\theta/2)\,|1\rangle$ is the parameterization of the qubit state $|\psi\rangle$ in terms of the zenithal $0 \leq \theta \leq \pi$ and azimuthal $0 \leq \phi < 2\pi$ angles of the said sphere, rotation and free evolution can be respectively employed to control at will the value of θ and ϕ.

In particular, we have implemented a selection of one-qubit logical gates: the CNOT, Hadamard, and Phase gates, which are key building-blocks in quantum algorithms. Input and output files as well as full details are found in SI. We assign the south $|1\rangle$ and north $|0\rangle$ poles of the Bloch sphere according to $|1\rangle \equiv |u_+\rangle$, $|0\rangle \equiv |u_-\rangle$. The initial condition is $\rho^0_{22} = 1$, $\rho^0_{11} = \rho^0_{12,r} = \rho^0_{12,i} = 0$, namely the qubit is initialized in its lowest energy state $|\psi\rangle = |u_-\rangle$, $\theta = 0$. The respective matrix representations $C(\epsilon)$, $H(\epsilon)$, $P(\gamma)$ of the CNOT, Hadamard, Phase gates in the ordered basis set $\{|1\rangle, |0\rangle\}$ are:

$$C(\epsilon) = \begin{pmatrix} 0 & {\rm e}^{i\epsilon} \\ {\rm e}^{-i\epsilon} & 0 \end{pmatrix} \quad H(\epsilon) = \begin{pmatrix} \frac{{\rm e}^{-i\epsilon}}{\sqrt{2}} & \frac{-{\rm e}^{-i\epsilon}}{\sqrt{2}} \\ \frac{1}{\sqrt{2}} & \frac{1}{\sqrt{2}} \end{pmatrix} \quad (7)$$

$$P(\gamma) = \begin{pmatrix} {\rm e}^{i\gamma} & 0 \\ 0 & 1 \end{pmatrix}$$

The angle $0 \leq \epsilon < 2\pi$ sets the direction of the rotation axis contained in the equatorial plane of the Bloch sphere. In $C(\epsilon)$, $H(\epsilon)$, the respective rotation angle around the mentioned axis is always π, $\pi/2$, and the rotation is implemented along the meridian $\phi = \pi - \epsilon$ determined by the selected ϵ value. The origin $\phi = 0$ is found at the positive $\mathbb{X}$ axis of the Bloch sphere, while $\epsilon = 0$ is located at its positive $\mathbb{Y}$ axis. We use the convention whereby positive increments in ϕ and ϵ correspond to anti clock-wise rotations in the equatorial plane -as defined by the perpendicular $\mathbb{X}$, $\mathbb{Y}$ axes- of the said sphere.

On the other hand, $\gamma = \phi_f - \phi_0$ -with $0 \leq \phi_0, \phi_f < 2\pi$ the initial and final azimuthal angles- is the rotation angle around the axis joining the poles $|1\rangle$ and $|0\rangle$ and along the parallel defined by the given θ value. The particular gates whose implementation we demonstrate are: the Pauli $X = C(\epsilon = 0)$, $Y = C(\epsilon = \pi/2)$ gates, the Hadamard $H(\epsilon = \pi/2)$, $H(\epsilon = 0)$ gates, and the $S = P(\gamma = -\pi/2)$, $T = P(\gamma = -\pi/4)$ gates. The action of the first four gates on the initial state $|\psi\rangle = |0\rangle$ is:

$$X\,|0\rangle = |1\rangle \quad Y\,|0\rangle = i\,|1\rangle \quad (8)$$

$$H\left(\frac{\pi}{2}\right)|0\rangle = \frac{1}{\sqrt{2}}(i\,|1\rangle + |0\rangle)$$

$$H(0)\,|0\rangle = \frac{1}{\sqrt{2}}(-\,|1\rangle + |0\rangle)$$

Note that S and T leaves $|0\rangle$ unaltered as $S\,|0\rangle = T\,|0\rangle = |0\rangle$. To show how $P(\gamma)$ can be employed to change ϕ, it is crucial to apply $P(\gamma)$ on qubit states with $\theta \neq 0, \pi$, namely different from $|0\rangle$ and $|1\rangle$. We choose $H(\pi)\,|0\rangle = (|1\rangle + |0\rangle)/\sqrt{2}$ for which $\theta = \pi/2$, $\phi = 0$, and the action of both S and T on it is:

$$S(H(\pi)\,|0\rangle) = \frac{1}{\sqrt{2}}(-i\,|1\rangle + |0\rangle) \quad (9)$$

$$T(H(\pi)\,|0\rangle) = \frac{1}{\sqrt{2}}\left(\frac{1-i}{\sqrt{2}}\,|1\rangle + |0\rangle\right)$$

If $|q\rangle$ is any of $X|0\rangle$, $Y|0\rangle$, $H(\pi/2)|0\rangle$, $H(0)|0\rangle$, $S(H(\pi)|0\rangle)$, $T(H(\pi)|0\rangle)$, the resulting density matrix $|q\rangle\langle q| = \overline{\rho}^f_{11}|1\rangle\langle 1| + (\overline{\rho}^f_{12,r} + i\overline{\rho}^f_{12,i})|1\rangle\langle 0| + (\overline{\rho}^f_{12,r} - i\overline{\rho}^f_{12,i})|0\rangle\langle 1| + \overline{\rho}^f_{22}|0\rangle\langle 0|$ in each case is:

$\|q\rangle\langle q\|$	$\overline{\rho}^f_{11}$	$\overline{\rho}^f_{22}$	$\overline{\rho}^f_{12,r}$	$\overline{\rho}^f_{12,i}$	θ	ϕ
$X\|0\rangle$	1	0	0	0	π	0
$Y\|0\rangle$	1	0	0	0	π	$\frac{\pi}{2}$
$H(\frac{\pi}{2})\|0\rangle$	$\frac{1}{2}$	$\frac{1}{2}$	0	$\frac{1}{2}$	$\frac{\pi}{2}$	$\frac{\pi}{2}$
$H(0)\|0\rangle$	$\frac{1}{2}$	$\frac{1}{2}$	$-\frac{1}{2}$	0	$\frac{\pi}{2}$	π
$S(H(\pi)\|0\rangle)$	$\frac{1}{2}$	$\frac{1}{2}$	0	$-\frac{1}{2}$	$\frac{\pi}{2}$	$-\frac{\pi}{2}$
$T(H(\pi)\|0\rangle)$	$\frac{1}{2}$	$\frac{1}{2}$	$\frac{1}{2\sqrt{2}}$	$-\frac{1}{2\sqrt{2}}$	$\frac{\pi}{2}$	$-\frac{\pi}{4}$

Table 1: Resulting density matrix $|q\rangle\langle q|$ with $|q\rangle$ being $X|0\rangle$, $Y|0\rangle$, $H(\pi/2)|0\rangle$, $H(0)|0\rangle$, $S(H(\pi)|0\rangle)$, $T(H(\pi)|0\rangle)$ (see main text).

To implement a general rotation in QBithm along a given meridian ϕ of the Bloch sphere with the aim of changing θ, some key parameters need to be set. First, one provides the desired g_J, $|\vec{\mathbf{B}}_1|$, $\omega_{\rm MW}/2\pi$ values in qbithm.f. We choose $g_J = 2$, $|\vec{\mathbf{B}}_1| = 1.5$ mT, $\omega_{\rm MW}/2\pi = \omega_{+-}/2\pi = 0.3$ cm^{-1} hence $\delta = 0$. The energies u_+, u_- to calculate ω_{+-} are taken by QBithm from qb.ddata. Then, the rotation gate is selected in qb.adata together with the particular ϵ value that gives rise to ϕ. The remaining parameter to be introduced in this input file is the rotation time Δt_i. If $\kappa > 0$ is the rotation angle, Δt_i is determined from the condition $\Omega_{\rm g}\Delta t_i = \kappa$. Particularly, if θ_0 and θ_f are the initial and final zenithal angles with $0 \leq \theta_0, \theta_f < 2\pi$; since QBithm rotations are clock-wise (see below), $\kappa = \theta_f - \theta_0$ when $\theta_f > \theta_0$ and $\kappa = 2\pi - (\theta_0 - \theta_f)$ when $\theta_0 > \theta_f$. We recommend first to use a dummy Δt_i value to compute $\Omega_{\rm g}$, then to read $\Omega_{\rm g}$ in qb.out, and last to run QBithm again but with the right Δt_i value.

Since the initial qubit state is $|\psi\rangle = |0\rangle$ where $\theta_0 = 0$, implementing the X, Y gates requires $\kappa = \pi - 0 = \pi$ to reach $\theta_f = \pi$, while $H(\pi/2)$, $H(0)$ require $\kappa = \pi/2 - 0 = \pi/2$ to get $\theta_f = \pi/2$. As the computed $\Omega_{\rm g}/2\pi$ is ≈ 21.0 MHz, the π rotation involved in the X, Y gates takes $\Delta t_\pi = \pi/\Omega_{\rm g} \approx 23.8$ ns, while the $\pi/2$ rotation that implements $H(\pi/2)$, $H(0)$ takes $\Delta t_{\pi/2} = (\pi/2)/\Omega_{\rm g} \approx 11.9$ ns.

On the other hand, to implement the action of the gate sequences $SH(\pi)$, $TH(\pi)$ on $|0\rangle$, two steps are required in qb.adata in each case. The first one is common and consists in a $\pi/2$ rotation to produce $H(\pi)$ with $\epsilon = \pi$ and $\Delta t_{\pi/2} \approx 11.9$ ns. At this moment, the qubit state $H(\pi)|0\rangle$ is contained in the equatorial plane of the Bloch sphere with $\theta = \pi/2$, $\phi_0 = 0$, and $\overline{\rho}_{11} = \overline{\rho}_{22} = 1/2$, $\overline{\rho}_{12,r} = 1/2$, $\overline{\rho}_{12,i} = 0$. The action of $P(\gamma)$ will be to rotate it an angle γ around the axis joining the poles $|1\rangle$ and $|0\rangle$ until $\phi_f = \phi_0 + \gamma$ while keeping $\theta = \pi/2$ constant.

$P(\gamma)$ is implemented by selecting a free evolution in qb.adata and the right evolution time Δt_i. Indeed, under free evolution, the spin undergoes Larmor precession around the $\vec{\mathbf{B}}$ direction with angular frequency ω_{+-}. After Δt_i, the qubit state is rotated the desired angle γ around the above-mentioned axis with θ unaltered. According to the fact that QBithm rotations are clock-wise, $\omega_{+-}\Delta t_i = -\gamma$ provides Δt_i when $\phi_f < \phi_0$, while $\omega_{+-}\Delta t_i = 2\pi - \gamma$ applies in case $\phi_f > \phi_0$. Since $\omega_{+-}/2\pi = 0.3$ cm^{-1}, the $\gamma = -\pi/2$ and $\gamma = -\pi/4$ rotations take $\Delta t_{-\pi/2} = (\pi/2)/\omega_{+-} \approx 0.028$ ns and $\Delta t_{-\pi/4} = (\pi/4)/\omega_{+-} \approx 0.014$ ns. Note that both $|\vec{\mathbf{B}}_1|$ and $\omega_{\rm MW}$ are automatically set to zero by QBithm when performing a free evolution and reset to the values provided in qbithm.f once the said evolution is done.

The obtainment of short $\Delta t_\gamma < 1$ ns values can be experimentally solved by extending the free evolution with a large enough number $m > 0$ of periods $2\pi/\omega_{+-}$ yet small enough to keep $\Delta t_\gamma + m2\pi/\omega_{+-}$ below the relaxation timescale thus not altering the desired final state. The convention $|1\rangle \equiv |u_+\rangle$, $|0\rangle \equiv |u_-\rangle$ coded in QBithm is the reason why both θ and ϕ rotations are clock-wise. E.g., this fact makes $H(\pi)$ -whose rotation axis $\epsilon = \pi$ is placed at the negative $\mathbb{Y}$ axis of the Bloch sphere- take $|0\rangle$ to $(|0\rangle + |1\rangle)/\sqrt{2}$ where $\phi = 0$ instead of $(|0\rangle - |1\rangle)/\sqrt{2}$ where $\phi = \pi$. In the opposite convention, one would use $\phi = \epsilon - \pi$ with the same ϵ values to produce the same rotated states up to a global phase.

We have run $X, Y, H(\pi/2), H(0), SH(\pi), TH(\pi)$ in QBithm as indicated above with $|0\rangle$ as the initial state and the resulting density matrices written in qb.out coincide with the expected ones of Table 1. Both X and Y inverts the population from $|0\rangle$ with $\rho^0_{22} = 1$, $\theta = 0$ to $\propto |1\rangle$ with $\overline{\rho}^f_{11} = 1$, $\theta = \pi$. The fact $\overline{\rho}^f_{11} = \overline{\rho}^f_{22} = 1/2$ indicates an equally-weighted superposition between $|0\rangle$ and $|1\rangle$ with $\theta = \pi/2$. Hence, the qubit is found in the equatorial plane

of the Bloch sphere. Since the action of S and T conserves the θ value, $\overline{\rho}^f_{11} = \overline{\rho}^f_{22} = 1/2$ remains.

All in all, given an initial qubit state on the Bloch sphere whose coordinates are (θ_0, ϕ_0), one can reach any other point (θ_f, ϕ_f) with $0 \leq \theta_0, \theta_f, \phi_0, \phi_f < 2\pi$. If $\theta_f \neq \theta_0$, the first step consists in a rotation with $\epsilon = \pi - \phi_0$ and $\Delta t_\kappa = (\theta_f - \theta_0)/\Omega_g$ when $\theta_f > \theta_0$ or $\Delta t_\kappa = (2\pi - (\theta_0 - \theta_f))/\Omega_g$ in case $\theta_f < \theta_0$. Then, if $\phi_f \neq \phi_0$, depending on whether $\phi_f < \phi_0$ or $\phi_f > \phi_0$, a free evolution is implemented with $\Delta t_\gamma = -\gamma/\omega_{+-}$ or $\Delta t_\gamma = (2\pi - \gamma)/\omega_{+-}$. Interestingly, one could use a single rotation axis $\epsilon = \epsilon_0$ and yet also reach any point (θ_f, ϕ_f) from (θ_0, ϕ_0). For instance, if $\epsilon_0 = 0$ which places the rotation axis at the positive $\mathbb{Y}$ axis of the Bloch sphere, one should first implement a free evolution until reaching $(\theta_0, \phi = \pi)$ when $\phi_0 \neq \pi$. Then, a rotation with the right Δt_κ around $\epsilon_0 = 0$ allows getting $(\theta_f, \phi = \pi)$. Last, a new free evolution transforms $\phi = \pi$ into ϕ_f.

The previous examples have been carried out under ideal circumstances, namely $\Gamma_{ab} = \Gamma_{em} = \Gamma_{mag} = \Gamma_{ab,add} = \Gamma_{em,add} = 0$ and $\Gamma_{mag,add} = 10^{-10}$ μs^{-1} as explained above, as well as $\delta = 0$ and the right values of ϵ, Δt_κ, Δt_γ. This setting excludes both relaxation and experimental imperfections, and allows following the qubit evolution in time as a point circulating on the Bloch sphere just by translating $\overline{\rho}^f$ written in qb.out in terms of θ and ϕ as done in Table 1. As soon as the rates become comparable or shorter than the gate/algorithm runtime, the qubit is rather described as a mixed state and cannot be followed as a pure state on the mentioned sphere nor $\overline{\rho}^f$ can be translated into θ, ϕ.

We now study how changes in the said ideal setting affect the implementation of X, $H(0)$, $SH(\pi)$. For that, we repeat the same examples by keeping $\Gamma_{ab} = \Gamma_{em} = \Gamma_{mag} = 0$ but with (i) $\delta = 0$, $\Gamma_{ab,add} = \Gamma_{em,add} = 0$, $\Gamma_{mag,add} > 0$, (ii) $\delta = 0$, $\Gamma_{mag,add} = 10^{-10}$ μs^{-1}, $\Gamma_{em,add} > 0$ with $T = 5$, 50, 200 K and $\Gamma_{ab,add}$ given by Eq.6, (iii) $\delta > 0$, $\Gamma_{ab,add} = \Gamma_{em,add} = 0$, $\Gamma_{mag,add} = 10^{-10}$ μs^{-1}, (iv) case of the $SH(\pi)$ gate sequence with $\delta = 0$, $\Gamma_{ab,add} = \Gamma_{em,add} = 0$, $\Gamma_{mag,add} = 10^{-10}$ μs^{-1} and increments relative to the right values $\epsilon = \pi$, $\Delta t_{\kappa=\pi/2} \approx 11.9$ ns, $\Delta t_{\gamma=-\pi/2} \approx 0.028$ ns. For each value (i) $\Gamma_{mag,add} > 0$, (ii) $\Gamma_{em,add} > 0$, (iii) $\delta > 0$ and increment (iv) in ϵ, $\Delta t_{\kappa=\pi/2}$, $\Delta t_{\gamma=-\pi/2}$, we obtain a density matrix $\overline{\sigma}^f$. The implementation of X, $H(0)$, $SH(\pi)$ under (i), (ii), (iii), (iv) is evaluated by computing the fidelity $0 \leq F = F(\overline{\rho}^f, \overline{\sigma}^f) \leq 1$ shown in Fig.1 with $\overline{\rho}^f$ in Table 1.

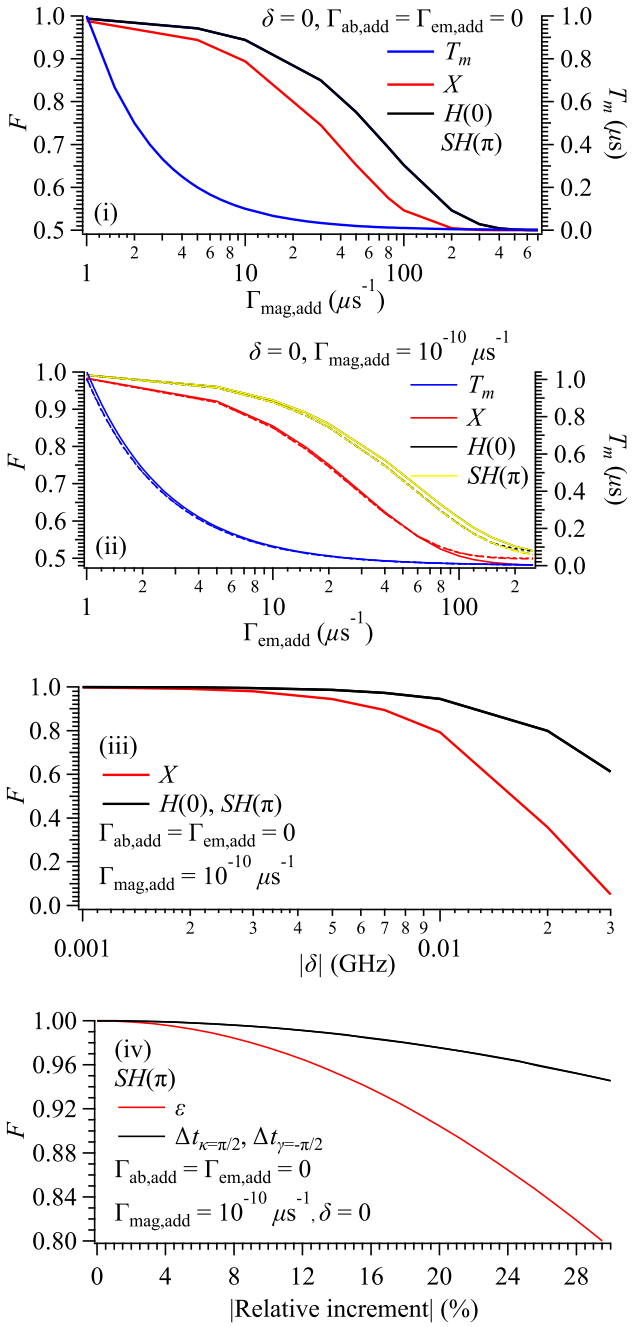

Figure 1: Computed F fidelities of X, $H(0)$, $SH(\pi)$ vs (i) $\Gamma_{mag,add}$, (ii) $\Gamma_{em,add}$, (iii) δ and (iv) increments in ϵ, $\Delta t_{\kappa=\pi/2}$, $\Delta t_{\gamma=-\pi/2}$ relative to π, ≈ 11.9 ns, ≈ 0.028 ns, resp.; with $\Gamma_{ab} = \Gamma_{em} = \Gamma_{mag} = 0$. (i) and (ii) also show the computed T_m. (ii): solid, dashed, dotted lines correspond to 5, 50, 200 K. $|\cdot|$ in (iii) and (iv) is the absolute value.

This assessment of the qubit performance when

realizing a given gate can be equally extended to the implementation of any digital one-spin-qubit algorithm, namely by calculating the fidelity between the ideal and non-ideal density matrices obtained after running the same gate sequence. In (i) and (ii), which can be respectively deemed as the limits where relaxation is driven only by the spin bath and only by the vibration bath, we also compute T_m to check how F and T_m compare with each other. High fidelities >95% require $T_m \gtrsim 0.89\ \mu s$ in (i) and $\gtrsim 0.94\ \mu s$ in (ii) with no experimental imperfections. The little affection by temperature in (ii) is due to $u_+ - u_- = 0.3\ \text{cm}^{-1} = 0.43$ K in the employed Eq.6 is small enough as compared to the explored temperatures 5, 50, 200 K. While $T_m \sim 1\ \mu s$ values are easily achievable by current spin qubits, the interest of our method is here rather found at determining the T_m that one would need to drive the spin qubit through the desired number of gates with the prescribed algorithm fidelity.

We also highlight the role of δ, ϵ, Δt_κ, Δt_γ as key design parameters since deviations from $\delta = 0$ and the right values of ϵ, Δt_κ, Δt_γ further lower F. As seen in (iii), a longer $\vec{\mathbf{B}}_1$-driven rotation -as the one producing X respect to the one involved in $H(0)$, $SH(\pi)$- leads to a lower F for a fixed δ and requires a smaller $|\delta|$ to achieve a given F. High fidelities $> 95\%$ are found with $|\delta| < 5$ MHz in X and $|\delta| < 10$ MHz in $H(0)$, $SH(\pi)$ if relaxation is negligible. On the other hand, (iv) shows that the fine tuning of ϵ requires more attention than that of Δt_κ, Δt_γ. The relative increment in ϵ must not exceed 14.5% to keep $F > 95\%$, while this high fidelity can already be obtained with relative increments in Δt_κ, Δt_γ below 28.5%. Note that $H(0)$, $SH(\pi)$ only differ in a free evolution. Since its runtime ≈ 0.028 ns is shorter enough than the explored $\Gamma^{-1}_{\text{mag,add}}$, $\Gamma^{-1}_{\text{em,add}}$ values and δ is always equal to the constant value ω_{+-} in any free evolution, the fidelities of $H(0)$, $SH(\pi)$ are virtually the same in (i), (ii), (iii).

Pulse sequences: Rabi oscillations and spin relaxation times

We study four potential molecular spin qubits as case studies defined from the energy schemes of the molecular coordination complexes in Fig.2: **(1)** $[\text{VO(dmit)}_2]^{2-}$, **(2)** $[\text{V(dmit)}_3]^{2-}$, **(3)** VOPc, **(4)** $[\text{Cu(mnt)}_2]^{2-}$. Diagonalization of Eq.5 and production of qb.ddata is conducted by SIMPRE with $J = 1/2$, $I(\text{V}^{4+}) = 7/2$, $I(\text{Cu}^{2+}) = 3/2$, $B^q_k \equiv 0$, $P \equiv 0$. The two qubit states $|m_J, m_I\rangle$ are the eigenstates $|-1/2, -1/2\rangle$, $|+1/2, -1/2\rangle$ in **(1)**-**(3)**, and $|-1/2, +3/2\rangle$, $|+1/2, +3/2\rangle$ in **(4)**. We employ QBithm to reproduce the experimentally-determined Rabi oscillations, T_1 and T_m, as well as the spin relaxation time T_{dd} measured when applying the so-called CPMG sequence to **(4)**. [66–69] Full details along with input and output files are found in SI.

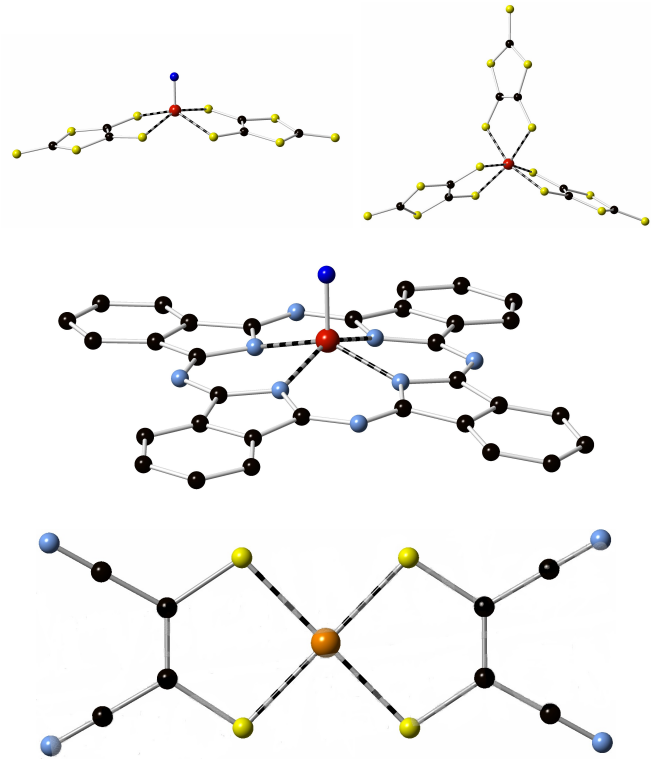

Figure 2: Molecular coordination complexes, with magnetic atomic ions V^{4+} (red) and Cu^{2+} (orange), as case studies of potential spin qubits. Top Left: **(1)**, Top Right: **(2)**, Middle: **(3)**, Bottom: **(4)**. C: black, S: yellow, N: pale blue, O: dark blue. [66–69]

The operation mode is that of combining the *ab initio* and semi-empirical modes. SIMPRE is requested to not generate qb.mdata nor write in qb.ddata the matrix elements M_{+-} required to compute Γ_{ab}, Γ_{em}, thus making QBithm set $\Gamma_{\text{ab}} = \Gamma_{\text{em}} = 0$. We do request SIMPRE to compute Γ_{mag}. All in all, QBithm is operated by employing $\Gamma_{\text{mag,add}} = 0$, Eq.6, and $\Gamma_{\text{em,add}}$ as the only free parameter. Our attention has been put in the master equation, hence we leave aside in our particular study of **(1)**-**(4)** the well-separated task of performing the *ab initio* calculation of Γ_{ab}, Γ_{em}.

This issue has been addressed over the last years with fruitful results and we refer the reader interested in using the purely *ab initio* mode to SI, the adapted version of SIMPRE, and the relevant contributions. [56–62,70–73] In case of operating under the said mode, QBithm connects in a natural way with them as their output is part of the input required to determine $\Gamma_{\rm ab}$, $\Gamma_{\rm em}$. Interestingly, whenever Eq.1 provides an accurate enough description of the given physical process, the values of $\Gamma_{\rm ab,add}$, $\Gamma_{\rm em,add}$, $\Gamma_{\rm mag,add}$ that result from fitting relevant experimental data under either the semi-empirical or the combined mode can be used as a benchmark to guide which additional mechanisms should be included in $\Gamma_{\rm ab}$, $\Gamma_{\rm em}$, $\Gamma_{\rm mag}$ until the values of these rates resemble those of $\Gamma_{\rm ab,add}$, $\Gamma_{\rm em,add}$, $\Gamma_{\rm mag,add}$.

Rabi oscillations. An important parameter that must firstly be determined is $|\vec{\mathbf{B}}_1|$. For each case study, we pick the experimental oscillation measured at the highest attenuation. Its Fourier transform provides the experimental generalized Rabi frequency $\Omega^{\rm exp}_{1,\rm g}$ which is attributed to a relative magnitude $|\vec{\mathbf{B}}_1|_{1,\rm rel}=1$. $|\vec{\mathbf{B}}_1|$ is varied in QBithm until $\Omega_{\rm g}$ of the calculated oscillation matches $\Omega^{\rm exp}_{1,\rm g}$ with an appropriate value $|\vec{\mathbf{B}}_1|_1$. If $|\vec{\mathbf{B}}_1|_{i,\rm rel}>1$ are the relative magnitudes of the remaining experimental oscillations, [66–69] their $|\vec{\mathbf{B}}_1|_i$ values are $|\vec{\mathbf{B}}_1|_i=|\vec{\mathbf{B}}_1|_1\cdot|\vec{\mathbf{B}}_1|_{i,\rm rel}$. The largest attenuation correspond to the smallest $|\vec{\mathbf{B}}_1|$, $\Omega^{\rm exp}_{\rm g}$ and vice versa. Then, we adjust $\Gamma_{\rm em,add}$ to reproduce in the calculated oscillation the time decay of the experimental one. Fig.3 shows the results of this method applied to **(1)**, **(2)**, while those of **(3)**, **(4)** are found in SI.

In Fig.3 Right, we observe the onset of a long-lived experimental oscillation at $\tau\sim 200$ ns with a well-defined $\Omega^{\rm exp}_{\rm HH,g}$ when employing $|\vec{\mathbf{B}}_1|=1.12$ mT to drive **(2)**. According to the Fourier transform, [66] $\Omega^{\rm exp}_{\rm HH,g}/2\pi=14.68$ MHz which coincides with the proton ^{1}H Larmor frequency $\omega_{^1\rm H}$ at the working magnetic field $|\vec{\mathbf{B}}|=345$ mT. The requirement for the emergence of the said long-lived oscillation -known as Hartmann-Hahn condition- is twofold: a nearby proton hyperfine-coupled to **(2)**, and to drive **(2)** with the attenuation that makes $\Omega^{\rm exp}_{\rm g}$ match $\omega_{^1\rm H}$ at the given $|\vec{\mathbf{B}}|$. Our theoretical model does not consider any explicit proton in Eq.5, hence it is unable to reproduce the long-lived oscillation.

The Fourier transform of each experimental oscillation i peaks at the relevant $\Omega^{\rm exp}_{i,\rm g}$ but, importantly, its non-negligible width $\Delta^{\rm exp}_{i,\rm g}$ shows that the observed oscillation is actually composed of a continuum of $\Omega^{\rm exp}_{\rm g}$. [66–69] Particularly, $\Delta^{\rm exp}_{\rm g}$ is further increased upon lowering the attenuation $A_{\rm MW}$. In case $\Delta^{\rm exp}_{\rm g}$ becomes large enough with a major contribution of several $\Omega^{\rm exp}_{\rm g}$, see **(3)** and **(4)** in SI, the calculated oscillation may not produce a satisfactory match with the experimental one in the whole nutation time since our theoretical model just provides a single $\Omega_{\rm g}$. In an improved version of this model, we would (i) treat $\{\Omega^{\rm exp}_{i,\rm g},\Delta^{\rm exp}_{i,\rm g}\}$ as a (normalized) probability distribution $P^i_d=P^i_d(\Omega^{\rm exp}_{\rm g})$, e.g. with a Lorentzian shape, (ii) sample a representative set $\{\Omega^{\rm exp}_{j,i,\rm g}\}_j$ from P^i_d, (iii) compute $\langle \mathrm{M}_z\rangle(\Omega^{\rm exp}_{j,i,\rm g})=\langle \mathrm{M}_z\rangle(\Omega^{\rm exp}_{j,i,\rm g},t_1)$ at each $\Omega^{\rm exp}_{j,i,\rm g}$, and (iv) use the average $\langle\overline{\mathrm{M}}^i_z\rangle(t_1)=\Sigma_j P^i_d(\Omega^{\rm exp}_{j,i,\rm g})\langle \mathrm{M}_z\rangle(\Omega^{\rm exp}_{j,i,\rm g},t_1)$ plotted vs t_1 to compare with the experimental oscillation. [74]

Note that the sole decrease of $A_{\rm MW}$ also produces a faster decay of the experimental Rabi oscillations. Here, the increasing values found for $\Gamma_{\rm em,add}$ (and $\Gamma_{\rm ab,add}$ via Eq.6) in each case study must be split into the constant contribution $\Gamma_{\rm vb}$ from the vibration bath and that from an additional effective rate $\Gamma_{\rm MW}$ that grows up as $A_{\rm MW}$ is reduced to recover the mentioned faster decay. The appropriate modeling of this fact, attributed to the static fluctuation of the microwave power, [69] would include an extra term in Eq.1 that should operate when $|\vec{\mathbf{B}}_1|\neq 0$ and should recover $\Gamma_{\rm MW}$, while $\Gamma_{\rm em,add}=\Gamma_{\rm vb}$.

T_1 and T_m. In case the last gate G_n of a sequence is a free evolution, we saw that the calculated $\langle \mathrm{M}_z\rangle(t_n)$ and $|\langle \mathrm{M}_{xy}\rangle(t_n)|$ as functions of Δt_n decay respectively with rates Γ_1 and Γ_1, Γ_2. However, let us recall that the plot of interest in the determination of relaxation times is $\langle \mathrm{M}_z\rangle(t_n)$ and $|\langle \mathrm{M}_{xy}\rangle(t_n)|$ vs $m\tau$, being $1\leq m\leq n$ the number of time intervals in the sequence -including Δt_n- whose duration $\tau:=\Delta t_i$ is variable. Hence, the actual decay rates of $\langle \mathrm{M}_z\rangle(t_n)$ and $|\langle \mathrm{M}_{xy}\rangle(t_n)|$ represented vs $m\tau$ are Γ_1/m and Γ_1/m, Γ_2/m, resp.

Whether $\langle \mathrm{M}_z\rangle(t_n)$ and $|\langle \mathrm{M}_{xy}\rangle(t_n)|$ are determined by running the same gate sequence or not, if $m=m_z=m_{xy}$, since Γ_1 and Γ_2 lie essentially within the same order of magnitude for predefined values of $\Gamma_{\rm a}$, $\Gamma_{\rm e}$, $\Gamma_{\rm m}$, we find that the calculated $\langle \mathrm{M}_z\rangle(t_n)$ and $|\langle \mathrm{M}_{xy}\rangle(t_n)|$ might decay with not very dissimilar

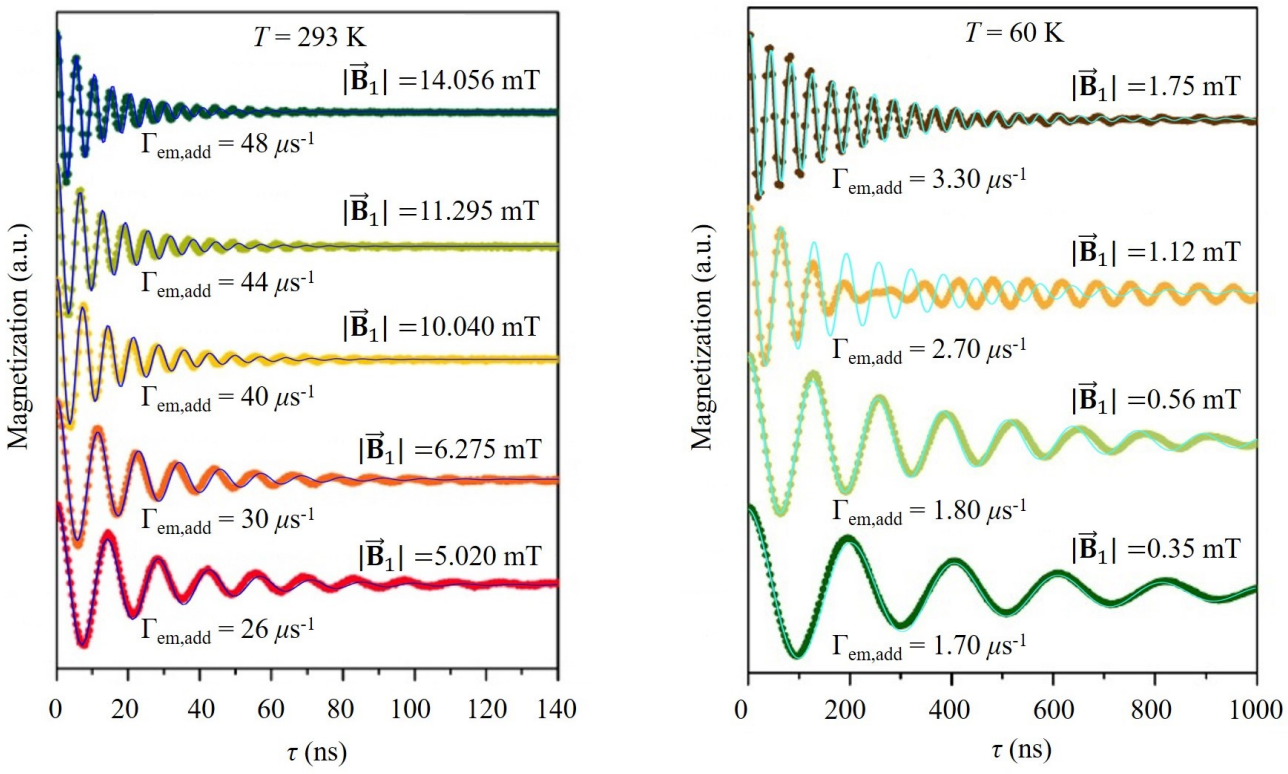

Figure 3: Experimental (dotted [66]) and calculated $\langle \mathrm{M}_z \rangle(t_1)$ (solid) magnetization vs nutation time τ, together with the $\Gamma_{\mathrm{em,add}}$ and $|\vec{\mathbf{B}}_1|$ values used in QBithm. Left: **(1)**. Right: **(2)**.

relaxation times vs $m\tau$. Moreover, when $m_z \neq m_{xy}$ -case of different sequences- with the same Γ_a, Γ_e, Γ_m, one may even learn that $\langle \mathrm{M}_z \rangle(t_n)$ decays faster than $|\langle \mathrm{M}_{xy} \rangle(t_n)|$ if $m_z < m_{xy}$. For instance, the respective use of $m_z = 1$ and $m_{xy} = 2$ in the Inversion recovery and Hahn sequence would lead to calculate $T_1 < T_m$ since $\Gamma_1 > \Gamma_1/2$, $\Gamma_2/2$ once Γ_1 and Γ_2 have the same magnitude as mentioned.

Herein, we will elaborate on the reasonable basis of modeling the implementation of each given sequence S_0 with its own working conditions W_0 as a unique physical process, hence characterized by a particular set of values $\{\Gamma^0_\mathrm{a}, \Gamma^0_\mathrm{e}, \Gamma^0_\mathrm{m}\}$ which may change as soon as either of S_0, W_0 is modified. As we already stated in a previous section, the target processes are the ones that might be captured by Eq.1. This would exclude those whose relaxation mechanisms are beyond the vibration and spin baths or, being driven only by them, produce stretched magnetization decays. The right description of these cases should proceed through the expansion of Eq.1 -even Eq.5- with relevant terms containing their own rates thus avoiding an artificial tuning of Γ_a, Γ_e, Γ_m. Once relaxation is covered by Eq.1 and these three rates, the change in Γ_a, Γ_e, Γ_m from one process to another may be due to the participation of a different set of mechanisms, or also to a variation in their magnitude if the set is the same. In case our Γ_ab, Γ_em, Γ_mag are conserved or do not include all mechanisms at play, the change in Γ_a, Γ_e, Γ_m and any missing contribution can still be collected by the additional rates $\Gamma_\mathrm{ab,add}$, $\Gamma_\mathrm{em,add}$, $\Gamma_\mathrm{mag,add}$.

This framework allows accommodating the specific fact that the experimental $\langle \mathrm{M}_z \rangle(t_n)$ and $|\langle \mathrm{M}_{xy} \rangle(t_n)|$ can also decay with rather different relaxation times when $m_z = m_{xy}$, even with $|\langle \mathrm{M}_{xy} \rangle(t_n)|$ decaying faster if $m_z < m_{xy}$. In general, we will model the computation of $\langle \mathrm{M}_z \rangle(t_n)$ and $|\langle \mathrm{M}_{xy} \rangle(t_n)|$ as two processes initially independent, each one with its own set of values $\{\Gamma^z_\mathrm{a}, \Gamma^z_\mathrm{e}, \Gamma^z_\mathrm{m}\}$ and $\{\Gamma^{xy}_\mathrm{a}, \Gamma^{xy}_\mathrm{e}, \Gamma^{xy}_\mathrm{m}\}$. In turn, this means to operate with the two sets of values $\{\Gamma^z_\mathrm{ab}, \Gamma^z_\mathrm{em}, \Gamma^z_\mathrm{mag}, \Gamma^z_\mathrm{ab,add}, \Gamma^z_\mathrm{em,add}, \Gamma^z_\mathrm{mag,add}\}$ and $\{\Gamma^{xy}_\mathrm{ab}, \Gamma^{xy}_\mathrm{em}, \Gamma^{xy}_\mathrm{mag}, \Gamma^{xy}_\mathrm{ab,add}, \Gamma^{xy}_\mathrm{em,add}, \Gamma^{xy}_\mathrm{mag,add}\}$. On the other hand, when we are interested in the same magnetization -either longitudi-

nal or in-plane- in different sequences $\{S_k\}_k$, we will also employ initially independent sets $\{\Gamma^k_{\rm ab}, \Gamma^k_{\rm em}, \Gamma^k_{\rm mag}, \Gamma^k_{\rm ab,add}, \Gamma^k_{\rm em,add}, \Gamma^k_{\rm mag,add}\}_k$. This approach would include the case of the CPMG sequence, which is parameterized in terms of the number k of refocusing π pulses.

As stated at the beginning of this section, our operation mode sets $\Gamma^{{\rm Rabi}/T_1/T_m/T_{dd}}_{\rm ab} = \Gamma^{{\rm Rabi}/T_1/T_m/T_{dd}}_{\rm em} = 0$ and binds $\Gamma^{{\rm Rabi}/T_1/T_m/T_{dd}}_{\rm ab,add}$ with $\Gamma^{{\rm Rabi}/T_1/T_m/T_{dd}}_{\rm em,add}$ via Eq.6. The models coded in SIMPRE for the computation of $\Gamma_{\rm mag}$ are devised to determine T_m, hence we use $\Gamma^{T_m}_{\rm mag} = \Gamma_{\rm mag}$. In addition, since this relaxation time also controls the decay rate of Rabi oscillations, we employed $\Gamma^{\rm Rabi}_{\rm mag} = \Gamma_{\rm mag}$. Once the spin bath is under consideration through $\Gamma^{T_m}_{\rm mag}$, $\Gamma^{\rm Rabi}_{\rm mag}$, we set $\Gamma^{T_m}_{\rm mag,add} = 0$ and use $\Gamma^{T_m}_{\rm em,add}$ as the only free parameter such as did with $\Gamma^{\rm Rabi}_{\rm mag,add}$ and $\Gamma^{\rm Rabi}_{\rm em,add}$. On the other hand, we reproduce T_1 by invoking only the vibration bath with $\Gamma^{T_1}_{\rm em,add}$ as the unique free parameter and $\Gamma^{T_1}_{\rm mag} = \Gamma^{T_1}_{\rm mag,add} = 0$. Whenever evidences reflect that T_1 is total or partially limited by the spin bath, the relevant contribution will be added to $\Gamma^{T_1}_{\rm mag,add}$. We lack an estimate for our case studies thus decide to fix $\Gamma^{T_1}_{\rm mag,add} = 0$ to avoid a second free parameter. The option $\Gamma^{T_1}_{\rm mag} = \Gamma_{\rm mag}$ must be excluded since the calculated $\Gamma_{\rm mag}$ values -intended for T_m- are too large to reproduce the long T_1 values measured at low temperatures. The use of $\Gamma^{T_m}_{\rm em,add}$ and $\Gamma^{T_1}_{\rm em,add}$ as free parameters fits our purpose of reproducing T_m and T_1 as a function of temperature since this is one of the key working conditions that modulates the contribution of the vibration bath to relaxation. The resulting $\Gamma^{T_m}_{\rm em,add}$ and $\Gamma^{T_1}_{\rm em,add}$ values produced at fitting the experimental T_m and T_1 of **(1)**-**(4)** as a function of temperature are found in SI.

CPMG sequence. This sequence is based on the building block $\{G_2 \to G_3 \to G_2\}$ which is repeated k times after an initial $\pi/2$ rotation G_1, namely $G_1 \to \{G_2 \to G_3 \to G_2\}_k$. G_2 is a free evolution with a variable duration time τ, while G_3 is a π rotation. Here, G_1 and G_3 are respectively performed along the positive $\mathbb{X}$ and $\mathbb{Y}$ axes of the Bloch sphere. All in all, the number of gates is $n = 3k+1$ where $m = 2k$ of them are run for the variable duration time τ. If we retake again the initial condition $\rho^0_{22} = 1$, $\rho^0_{11} = \rho^0_{12,r} = \rho^0_{12,i} = 0$, G_1 brings the qubit to an equally-weighted superposition between $|0\rangle$ and $|1\rangle$ in the equatorial plane of the Bloch sphere from the initial state $|0\rangle \equiv |u_-\rangle$. Given k, $|\langle {\rm M}_{xy}\rangle(t_{3k+1})|$ is plotted vs $2k\tau$ to extract the spin relaxation time T_{dd} after fitting the said representation to an exponential decaying curve $f(2k\tau) = a + b\exp(-2k\tau/T_{dd})$. The key to CPMG sequence is the continual implementation of $\{G_2 \to G_3 \to G_2\}$ which mitigates the relaxation produced by the spin bath and lengthen T_{dd} as k is increased. [69] In practice, T_{dd} is limited by experimental imperfections.

The CPMG sequence is run at a fixed temperature. In addition, since its role is to act essentially on the spin bath, we model the lengthening of T_{dd} as a reduction in $\Gamma^{T_{dd}}_{\rm mag,add}$ with a constant $\Gamma^{T_{dd}}_{\rm em,add} = \Gamma^{T_{dd},{\rm lim}}_{\rm em,add}$. $\Gamma^{T_{dd}}_{\rm mag}$ is here set to zero thus the entire relaxation due to the spin bath will be collected by $\Gamma^{T_{dd}}_{\rm mag,add}$ as a free parameter. We determine $\Gamma^{T_{dd},{\rm lim}}_{\rm em,add}$ by fitting the calculated T_{dd} to the limiting value $T^{\rm lim}_{dd}$ measured at a high enough $k_{\rm lim}$. Since the qubit is already certainly decoupled from the spin bath at $k = k_{\rm lim}$, we employ $\Gamma^{T_{dd}}_{\rm mag,add} = 0$ in this particular fitting process. The $\Gamma^{T_{dd},{\rm lim}}_{\rm em,add}$ value would also contain an effective rate associated to experimental imperfections. Then, for each $k < k_{\rm lim}$ explored, we keep $\Gamma^{T_{dd}}_{\rm em,add} = \Gamma^{T_{dd},{\rm lim}}_{\rm em,add}$ and vary $\Gamma^{T_{dd}}_{\rm mag,add}$ until reproducing the experimental T_{dd}. The resulting $\Gamma^{T_{dd}}_{\rm mag,add}$ takes progressively lower values as k is increased and becomes zero for $k \geq k_{\rm lim}$. In the case of **(4)**, we lack $T^{\rm lim}_{dd}$. Hence, to illustrate our method, we use $T^{\rm lim}_{dd} = 1.4$ ms obtained with the largest $k = 2048$ implemented. We get $\Gamma^{T_{dd},{\rm lim}}_{\rm em,add} = 7.31{\cdot}10^{-4}\ \mu{\rm s}^{-1}$ and the $\Gamma^{T_{dd}}_{\rm mag,add}$ found to fit the experimental T_{dd} for each $k = 1$, 8, 32, 128, 256, 512, 1024, 2048 is depicted in Fig.4.

The oscillatory decay of the experimental magnetization curves in [69] is not present in the computed $|\langle {\rm M}_{xy}\rangle(t_{3k+1})|$ shown in Fig.4 since our theoretical model does not include the interaction between the molecular spin and nearby nuclear spins as explained in a previous section. We also note that Hahn and CPMG sequences coincide for $k = 1$ so $T_m = T_{dd}$. Our method described above delivers $\Gamma^{T_m}_{\rm em,add} \approx 0.15\ \mu{\rm s}^{-1}$ when applied to **(4)** in SI to reproduce the experimental $T_m = 6.8\ \mu$s with $\Gamma^{T_m}_{\rm mag} = \Gamma_{\rm mag} \approx 2.6 \cdot 10^{-3}\ \mu{\rm s}^{-1}$ fixed in qb.ddata. The fact that we employ a value $\Gamma^{T_m}_{\rm em,add} \approx 0.15\ \mu{\rm s}^{-1} \gg \Gamma^{T_{dd},{\rm lim}}_{\rm em,add}$ needed to compensate the rather small

$\Gamma_{\rm mag} \approx 2.6 \cdot 10^{-3}$ μs^{-1} as compared to $\Gamma^{T_{dd}}_{\rm mag,add} \approx 0.15$ μs^{-1} found for $k = 1$ points towards an underestimated $\Gamma_{\rm mag}$.

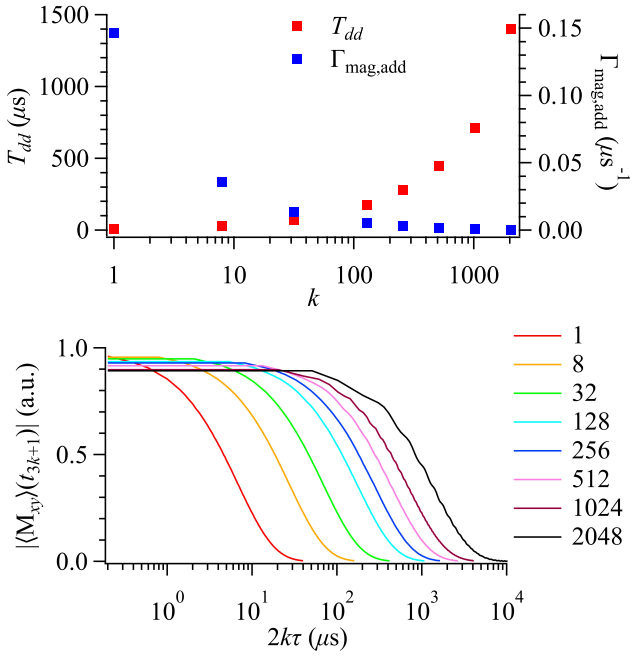

Figure 4: Top: $\Gamma_{\rm mag,add}$ rates determined with QBithm to fit the experimental spin relaxation times T_{dd} measured when applying the CPMG sequence to **(4)** with $k = 1$, 8, 32, 128, 256, 512, 1024, 2048 π rotations. [69] Bottom: computed in-plane magnetization curves at each $\Gamma_{\rm mag,add}$ value above.

Discussion

Over the last decade, the study of the relaxation times T_1 and T_m has undoubtedly produced a body of design principles aimed at quenching the loss of quantum information stored in freely-evolving spin qubits. At this point, these well-established strategies that have resulted from a fruitful interplay theory-experiment set an ideal position for pushing towards the use of spin qubits in quantum algorithms as one of their key applications. This means to submit the qubit to an evolution which is not free anymore but rather driven by the user while relaxation and imperfections are likewise active. Within this widened picture, T_1 and T_m -intended for free evolution- provide a rather limited benchmark for the qubit performance might now be evaluated after running the selected algorithm of interest in the form of fidelity as the actual figure of merit.

We have posed and conducted the analytical resolution of a master equation devoted to run any one-spin-qubit algorithm set and driven by the user as a gate sequence subject to relaxation and experimental imperfections. The fidelity F is easily computed by combining the two qubit density matrices obtained after running the algorithm of interest with and without relaxation rates Γ and imperfections. This allows assessing a given spin qubit among several algorithms as well as comparing different spin qubits each one implementing the same algorithm. The master equation is operated through the software package QBithm which, in addition to show the time evolution of the density matrix, also offers the possibility of calculating longitudinal and in-plane magnetization curves to determine relaxation times such as T_1 and T_m, ESE-detected spectra, and Rabi oscillations. Interestingly, this feature helps to translate between T_m and F in a given algorithm run by a spin qubit: one can learn either what F would result from the Γ values that reproduce T_m, or which the minimum T_m should be so the consequent Γ values lead to a prescribed F.

The operation mode in QBithm depends on the inputted Γ values whether they are previously calculated or employed as free parameters. In the first case, our work takes up the torch from those efforts devoted to design *ab initio* methods for computing the rates Γ which now feed QBithm. On the other hand, when using Γ to fit experimental data, the resulting values can serve as a benchmark for the above-mentioned methods. Here, we have operated under a rather combined mode that allows dealing with a plethora of potential case studies and experiments of wide interest. In particular, we managed to reproduce the measured experimental data by describing the initially-complex issue of relaxation -such as that originated in the vibration bath- with realistic values of a single relaxation rate as the only free parameter. At this point, the ball is now in the court of those researchers interested in proceeding through the purely *ab initio* operation mode.

As a function test, we did compute $\Gamma_{\rm ab}$ and $\Gamma_{\rm em}$ for **(4)** from its calculated molecular-vibration spectrum published in [70]. The obtained values $< 10^{-10}$ μs^{-1} in the range $5-300$ K are rather negligible and cannot account for the experimental T_1 and T_m lying inside 1 μs $-$ 100 ms. We find that key to those such a low values is the mismatch between the spin-

qubit gap $\omega_{+-} \sim 0.3$, ~ 1.0 cm^{-1} -depending on whether the X or the Q band is employed- and the harmonic frequencies $\omega_i \gtrsim 20$ cm^{-1} of the molecular vibrations, as well as the low phonon populations that ω_i produce at the working temperatures. In particular, we state that calculated vibration spectra should also include the low-energy lattice vibrations -specially those with $\omega_i \lesssim 1$ cm^{-1}- for a proper description of the direct relaxation process between the two states $|u_+\rangle$ and $|u_-\rangle$ of spin qubits. [75, 76] Indeed, after resetting ω_i to 1 cm^{-1} and by assuming that both spin-vibration matrix elements and reduced masses remain unaltered, we found that each molecular vibration contributes to $\Gamma_{\rm ab}$, $\Gamma_{\rm em}$ with values $\sim 10^6 - 10^8$ times larger in $5 - 300$ K. Hence, if $\sim 10 - 100$ lattice vibrations with $\omega_i \lesssim 1$ cm^{-1} were included, $\Gamma_{\rm ab}$ and $\Gamma_{\rm em}$ would increase by $\sim 10^7 - 10^{10}$ thus resulting in more realistic values in the μs scale and longer.

Molecular/local vibrations should not, however, be discarded as they can play a significant role in Raman relaxation processes. [77] Given two vibration modes i, j -either $i = j$ or $i \neq j$-, the mismatch of ω_i, ω_j respect to ω_{+-} is not crucial since the resonance condition to fulfil now is $|\omega_i - \omega_j| \sim \omega_{+-}$. While this condition suffices to account for virtual Raman processes, where the virtual intermediate state is either above u_+ or below u_- in energy, real Raman processes additionally require an eigenstate $|u_c\rangle$ of the relevant spin Hamiltonian as the intermediate state -with energy either $u_c > u_+$ or $u_c < u_-$- such that each $|u_c - u_+|$, $|u_c - u_-|$ must be similar to one among ω_i, ω_j.

In the case of **(1)-(4)**, the sole inclusion of the ground J, I quantum numbers in Eq.5 provides an energy scheme of $(2J+1)(2I+1)$ eigenstates that span no more than 1 cm^{-1}. Hence, $|u_c - u_+|$, $|u_c - u_-| \lesssim 1$ cm^{-1}. While this fact also supports the need of incorporating lattice vibrations with $\omega_i \lesssim 1$ cm^{-1}, molecular vibrations -having $\omega_i \gtrsim 20$ cm^{-1}- will play a significant role only if there exist $|u_c\rangle$ of high-enough energy such that $|u_c - u_+|$, $|u_c - u_-| \gtrsim 20$ cm^{-1}. Thus, for a proper description of molecular/local-vibration relaxation in spin qubits, we also state that one could require to expand Eq.5 with excited J quantum numbers or even with other degrees of freedom which also couple to J and produce states that might also work as high-energy intermediate states. As included in our theoretical model, both real and virtual Raman processes can also proceed through intermediate states with an energy between u_- and u_+, being the resonance condition $\omega_i + \omega_j \sim \omega_{+-}$. Since $\omega_{+-} \lesssim 1$ cm^{-1}, the proper modeling of this relaxation case would require again the participation of low-energy lattice vibrations.

QBithm can readily deal with the required expansion $\hat{H}'$ of Eq.5 since, as mentioned in **QBithm software package**, one can request $\Gamma_{\rm ab} = \Gamma_{\rm em} = 0$ within the *ab initio* operation mode and input in $\Gamma_{\rm ab,add}$ and $\Gamma_{\rm em,add}$ the values externally calculated with $\hat{H}'$. In this case, one sets $(2J+1)(2I+1) = 2$ in qbithm.f and manually writes in qb.ddata the values of u_-, u_+, N_{+-} computed also with $\hat{H}'$. In addition, SIMPRE can be fed with vibrations of any frequency range, both lattice- and molecular-like; hence, the calculated $\Gamma_{\rm ab}$, $\Gamma_{\rm em}$ can already account for the full direct relaxation process with Eq.5 and $\Gamma_{\rm ab,add} = \Gamma_{\rm em,add} = 0$ since the description of this process only needs to invoke $|u_-\rangle$ and $|u_+\rangle$ but not any intermediate state.

On the other hand, beside the production of high-fidelity gates, the importance of a small detuning $\delta = \omega_{+-} - \omega_{\rm MW}$ also manifests itself in the implementation of pulse sequences, e.g. those employed to determine T_1, T_m and produce Rabi oscillations as we check in SI. Despite $\delta \neq 0$, one can still conduct a faithful driving with less stringent upper bounds in $|\delta|$ if ω_{+-} lies inside the excitation bandwidth $\mathrm{B} = [\omega_{\rm MW} - \Delta\omega_{\rm MW}/2, \omega_{\rm MW} + \Delta\omega_{\rm MW}/2]$. For pulses at least 10 ns long as the ones employed by us, $\Delta\omega_{\rm MW} \leq 100$ MHz in standard EPR setups. Moreover, the distribution D of the spin Hamiltonian parameters as a result of static disorder leads to a broadening in ω_{+-} whose FWHM can be as high as 300 MHz. [78] Hence, there exists a window as wide as $\Delta\omega_{\rm MW}/2 + \mathrm{FWHM}/2 = 200$ MHz where the tails of B and D can significantly overlap provided $|\delta| < 200$ MHz. This is the case of **(1)-(4)**, where the minimum detuning $|\delta|_{\rm min}$ ranges from 10 to 150 MHz. Instead of including $\Delta\omega_{\rm MW}$ and the mentioned FWHM in our calculations, and since the resonance probability decays abruptly as soon as $|\delta|$ becomes larger, we have opted for a simpler alternative which effectively covers the relevant physics. Namely, for each case study we work out with the $|\vec{\mathbf{B}}|$ direction $\vec{\mathbf{u}}$ where $|\delta| = |\delta|_{\rm min}$ and set $\omega_{\rm MW}$ in qbithm.f with the value of ω_{+-} corresponding to

$\vec{\mathbf{u}}$. If there exist several $\vec{\mathbf{u}}$ directions, e.g. in systems with some isotropy, one would integrate the relevant magnetization curve over all $\vec{\mathbf{u}}$ as it may happen in powder samples and frozen solutions (see SI for more details).

All in all, our contribution comes with an assorted toolkit that tackles the issue of driving one spin qubit on the Bloch sphere while exposed to relaxation, thus supplying the complementary piece of those design principles devised to lengthen T_m for a spin in free evolution. A natural next step for QBithm would be the expansion of the computational Hilbert space $\{|u_+\rangle, |u_-\rangle\}$ to firstly accommodate two spin qubits and then a larger set of them to run more sophisticated gate-based algorithms. The first movement results in the implementation of two-qubit gates and the testing of their fidelity, [79] but also allows including physical processes not collected in our current theoretical model. Indeed, the said expansion could also consist in the interaction between a single qubit and a nearby nuclear spin-1/2 which is commonly behind some long-lived Rabi oscillations and the oscillatory behavior of some decaying magnetization curves.

Instead, the inclusion of other processes could require the addition of extra terms in the master equation, e.g. those ones that lead to the faster decay of Rabi oscillations upon increasing the microwave power or to the stretched shape of some magnetization curves. In case of existing evidence, longitudinal magnetization curves M_z with an stretch factor x below 1 are often interpreted as the sum of two non-stretched and exponentially-decaying curves, where one corresponds to a process operating on a shorter timescale and the other one on a longer one. This particular situation can still be addressed by QBithm provided both processes are described with two different sets of relaxation rates such as we do for **(1)-(4)** in SI. On the other hand, our calculated in-plane magnetization curves M_{xy}, which contain two decay rates Γ_1 and Γ_2, can exhibit an stretched shape with $x < 1$ provided $\Gamma_1 \neq \Gamma_2$. Hence, our model could also describe stretched M_{xy} curves with $x < 1$ if the origin of this fact is the participation of the vibration bath, since $\Gamma_a + \Gamma_e \neq 0$ is the condition that leads to $\Gamma_1 \neq \Gamma_2$.

QBithm also offers an appealing opportunity for experimentalists. In addition to the possibility of studying imperfections, such as deviations from ideal gate time and angle ϵ as studied in Fig.1, it also encourages to conduct better-characterized experiments in terms of parameters key for QBithm. These include δ, $|\vec{\mathbf{B}}_1|$, the polarization angle α of $\vec{\mathbf{B}}_1$, and even ϵ. Moreover, the effective Hamiltonian in Eq.2 could be modified to implement the potential option of driving the spin via an oscillating electric field as already experimentally explored with success. [80] In a nutshell, we expect that our work will be of help to the wide community of spin qubits and to those researchers interested in exploiting this physical platform for quantum information and computation.

References

[1] B. Bauer, S. Bravyi, M. Motta, G. Kin-Lic Chan, Quantum Algorithms for Quantum Chemistry and Quantum Materials Science. *Chem. Rev.* **120**, 12685–12717 (2020).

[2] K. Head-Marsden, J. Flick, C. J. Ciccarino, P. Narang, Quantum Information and Algorithms for Correlated Quantum Matter. *Chem. Rev.* **121**, 3061–3120 (2021).

[3] L. Henriet, L. Beguin, A. Signoles, T. Lahaye, A. Browaeys, G.-Olivier Reymond, C. Jurczak, Quantum computing with neutral atoms. *Quantum* **4**, 327 (2020).

[4] B. Lekitsch, S. Weidt, A. G. Fowler, K. Mølmer, S. J. Devitt, C. Wunderlich, W. K. Hensinger, Blueprint for a microwave trapped ion quantum computer. *Sci. Adv.* **3**, 2 (2017).

[5] X. Liu, M. C. Hersam, 2D materials for quantum information science. *Nat. Rev. Mater.* **4**, 669–684 (2019).

[6] A. J. Heinrich, W. D. Oliver, L. M. K. Vandersypen, A. Ardavan, R. Sessoli, D. Loss, A. B. Jayich, J. Fernández-Rossier, A. Laucht, A. Morello, Quantum-coherent nanoscience. *Nat. Nanotechnol.* **16**, 1318–1329 (2021).

[7] C.-Jui Yu, S. von Kugelgen, D. W. Laorenza, D. E. Freedman, A Molecular Approach to Quantum Sensing. *ACS Cent. Sci.* **7**, 712–723 (2021).

[8] D. W. Laorenza, D. E. Freedman, Could the Quantum Internet Be Comprised of Molecular Spins with Tunable Optical Interfaces? *J. Am. Chem. Soc.* **144**, 21810-21825 (2022).

[9] A. Laucht et al., Roadmap on quantum nanotechnologies. *Nanotechnology* **32**, 162003 (2021).

[10] D. S. Wang, M. Haas, P. Narang, Quantum Interfaces to the Nanoscale. *ACS Nano* **15**, 7879–7888 (2021).

[11] L. Schlipf, T. Oeckinghaus, K. Xu, D. B. R. Dasari, A. Zappe, F. F. de Oliveira, B. Kern, M. Azarkh, M. Drescher, M. Ternes, K. Kern, J. Warchtrup, A. Finkler, A molecular quantum spin network controlled by a single qubit. *Sci. Adv.* **3**, (2017).

[12] D. D. Awschalom, R. Hanson, J. Wrachtrup, B. B. Zhou, Quantum technologies with optically interfaced solid-state spins. *Nat. Photonics* **12**, 516–527 (2018).

[13] M. T. Madzik, S. Asaad, A. Youssry, B. Joecker, K. M. Rudinger, E. Nielsen, K. C. Young, T. J. Proctor, A. D. Baczewski, A. Laucht, V. Schmitt, F. E. Hudson, K. M. Itoh, A. M. Jakob, B. C. Johnson, D. N. Jamieson, A. S. Dzurak, C. Ferrie, R. Blume-Kohout, A. Morello, Precision tomography of a three-qubit donor quantum processor in silicon. *Nature* **601**, 348–353 (2022).

[14] M. Atzori, R. Sessoli, The Second Quantum Revolution: Role and Challenges of Molecular Chemistry. *J. Am. Chem. Soc.* **141**, 11339–11352 (2019).

[15] E. Coronado, Molecular magnetism: from chemical design to spin control in molecules, materials and devices. *Nat. Rev. Mater.* **5**, 87–104 (2020).

[16] M. R. Wasielewski et al., Exploiting chemistry and molecular systems for quantum information science. *Nat. Rev. Chem.* **4**, 490–504 (2020).

[17] F. Luis, P. J. Alonso, O. Roubeau, V. Velasco, D. Zueco, D. Aguilà, J. I. Martínez, L. A. Barrios, G. Aromí, A dissymmetric [Gd2] coordination molecular dimer hosting six addressable spin qubits. *Commun. Chem.* **3**, 176 (2020).

[18] I. Borilovic, O. Roubeau, B. Le Guennic, J. van Slageren, S. Lenz, S. J. Teat, G. Aromí, Three individually addressable spin qubits in a single molecule. *Chem. Commun.* **58**, 7530-7533 (2022).

[19] I. Gimeno, A. Urtizberea, J. Román-Roche, D. Zueco, A. Camón, P. J. Alonso, O. Roubeau, F. Luis, Broad-band spectroscopy of a vanadyl porphyrin: a model electronuclear spin qudit. *Chem. Sci.* **12**, 5621-5630 (2021).

[20] H. Biard, E. Moreno-Pineda, M. Ruben, E. Bonet, W. Wernsdorfer, F. Balestro, Increasing the Hilbert space dimension using a single coupled molecular spin. *Nat. Commun.* **12**, 4443 (2021).

[21] M. Chizzini, L. Crippa, A. Chiesa, F. Tacchino, F. Petiziol, I. Tavernelli, P. Santini, S. Carretta, Molecular nanomagnets with competing interactions as optimal units for qudit-based quantum computation. *Phys. Rev. Research* **4**, 043135 (2022).

[22] C. Godfrin, S. Thiele, A. Ferhat, S. Klyatskaya, M. Ruben, W. Wernsdorfer, F. Balestro, Electrical Read-Out of a Single Spin Using an Exchange-Coupled Quantum Dot. *ACS Nano* **11**, 3984–3989 (2017).

[23] G. Czap, P. J. Wagner, F. Xue, L. Gu, J. Li, J. Yao, R. Wu, W. Ho, Probing and imaging spin interactions with a magnetic single-molecule sensor. *Science* **364**, 6441 (2019).

[24] S. L. Bayliss, D. W. Laorenza, P. J. Mintun, B. D. Kovos, D. E. Freedman, D. D. Awschalom, Optically addressable molecular spins for quantum information processing. *Science* **370**, 1309-1312 (2020).

[25] P. Willke, T. Bilgeri, X. Zhang, Y. Wang, C. Wolf, H. Aubin, A. Heinrich, T. Choi, Coherent Spin Control of Single Molecules on a Surface. *ACS Nano* **15**, 17959–17965 (2021).

[26] J. N. Nelson, J. Zhang, J. Zhou, B. K. Rugg, M. D. Krzyaniak, M. R. Wasielewski, CNOT gate operation on a photogenerated molecular

electron spin-qubit pair. *J. Chem. Phys.* **152**, 014503 (2020).

[27] C. A. Collett, P. Santini, S. Carretta, J. R. Friedman, Constructing clock-transition-based two-qubit gates from dimers of molecular nanomagnets. *Phys. Rev. Research* **2**, 032037(R) (2020).

[28] I. Borilovic, P. J. Alonso, O. Roubeau, G. Aromí, A bis-vanadyl coordination complex as a 2-qubit quantum gate. *Chem. Commun.* **56**, 3139-3142 (2020).

[29] A. Gómez-León, Multiqudit interactions in molecular spins. *Phys. Rev. A* **106**, 022609 (2022).

[30] A. Ullah, Z. Hu, J. Cerdà, J. Aragó, A. Gaita-Ariño, Electrical two-qubit gates within a pair of clock-qubit magnetic molecules. *npj Quantum Inf.* **8**, 133 (2022).

[31] Y. Fu, Y. Wu, Y. Dai, X. Qin, X. Rong, J. Du, Molecular-Spin-Qubit Noise Spectroscopy Through Dynamical Decoupling. *Phys. Rev. Applied* **15**, L061001 (2021).

[32] T. Shibata, S. Yamamoto, S. Nakazawa, E. H. Lapasar, K. Sugisaki, K. Maruyama, K. Toyota, D. Shiomi, K. Sato, T. Takui, Molecular Optimization for Nuclear Spin State Control via a Single Electron Spin Qubit by Optimal Microwave Pulses: Quantum Control of Molecular Spin Qubits. *Appl. Magn. Reson.* **53**, 777–796 (2022).

[33] A. Castro, A. G. Carrizo, S. Roca, D. Zueco, F. Luis, Optimal Control of Molecular Spin Qudits. *Phys. Rev. Applied* **17**, 064028 (2022).

[34] A. Urtizberea, E. Natividad, P. J. Alonso, L. Pérez-Martínez, M. A. Andrés, I. Gascón, I. Gimeno, F. Luis, O. Roubeau, Vanadyl spin qubit 2D arrays and their integration on superconducting resonators. *Mater. Horiz.* **7**, 885-897 (2020).

[35] S. Carretta, D. Zueco, A. Chiesa, A. Gómez-León, F. Luis, A perspective on scaling up quantum computation with molecular spins. *Appl. Phys. Lett.* **118**, 240501 (2021).

[36] S. Lenz, D. König, D. Hunger, J. van Slageren, Room-Temperature Quantum Memories Based on Molecular Electron Spin Ensembles. *Adv. Mater.* **33**, 2101673 (2021).

[37] E. Garlatti, T. Guidi, S. Ansbro, P. Santini, G. Amoretti, J. Ollivier, H. Mutka, G. Timco, I. J. Vitorica-Yrezabal, G. F. S. Whitehead, R. E. P. Winpenny, S. Carretta, Portraying entanglement between molecular qubits with four-dimensional inelastic neutron scattering. *Nat. Commun.* **8**, 14543 (2021).

[38] C. Godfrin, A. Ferhat, R. Ballou, S. Klyatskaya, M. Ruben, W. Wernsdorfer, F. Balestro, Operating Quantum States in Single Magnetic Molecules: Implementation of Grover's Quantum Algorithm. *Phys. Rev. Lett.* **119**, 187702 (2017).

[39] M. Atzori, A. Chiesa, E. Morra, M. Chiesa, L. Sorace, S. Carretta, R. Sessoli, A two-qubit molecular architecture for electron-mediated nuclear quantum simulation. *Chem. Sci.* **9**, 6183-6192 (2018).

[40] F. Petiziol, M. Sameti, S. Carretta, S. Wimberger, F. Mintert, Quantum Simulation of Three-Body Interactions in Weakly Driven Quantum Systems. *Phys. Rev. Lett.* **126**, 250504 (2021).

[41] S. Chicco, A. Chiesa, G. Allodi, E. Garlatti, M. Atzori, L. Sorace, R. de Renzi, R. Sessoli, S. Carretta, Controlled coherent dynamics of [VO(TPP)], a prototype molecular nuclear qudit with an electronic ancilla. *Chem. Sci.* **12**, 12046-12055 (2021).

[42] M. Chizzini, L. Crippa, L. Zaccardi, E. Macaluso, S. Carretta, A. Chiesa, P. Santini, Quantum error correction with molecular spin qudits. *Phys. Chem. Chem. Phys.* **24**, 20030-20039 (2022).

[43] A. Chiesa, F. Petiziol, M. Chizzini, P. Santini, S. Carretta, Theoretical Design of Optimal Molecular Qudits for Quantum Error Correction. *J. Phys. Chem. Lett.* **13**, 6468-6474 (2022).

[44] D. Aravena, E. Ruiz, Spin dynamics in single-molecule magnets and molecular qubits. *Dalton Trans.* **49**, 9916-9928 (2020).

[45] R. Mirzoyan, N. P. Kazmierczak, R. G. Hadt, Deconvolving Contributions to Decoherence in Molecular Electron Spin Qubits: A Dynamic Ligand Field Approach. *Chem. Eur. J.* **27**, 9482-9494 (2021).

[46] A. Lunghi, S. Sanvito, Computational design of magnetic molecules and their environment using quantum chemistry, machine learning and multiscale simulations. *Nat. Rev. Chem.* **6**, 761–781 (2022).

[47] S. Cardona-Serra, L. Escalera-Moreno, J. J. Baldoví, A. Gaita-Ariño, J. M. Clemente-Juan, E. Coronado, SIMPRE1.2: Considering the hyperfine and quadrupolar couplings and the nuclear spin bath decoherence. *J. Comput. Chem.* **37**, 1238-1244 (2016).

[48] S. Lenz, K. Bader, H. Bamberger, J. van Slageren, Quantitative prediction of nuclear-spin-diffusion-limited coherence times of molecular quantum bits based on copper(II). *Chem. Commun.* **53**, 4477 (2017).

[49] L. Escalera-Moreno, A. Gaita-Ariño, E. Coronado, Decoherence from dipolar interspin interactions in molecular spin qubits. *Phys. Rev. B* **100**, 064405 (2019).

[50] A. Lunghi, S. Sanvito, Electronic spin-spin decoherence contribution in molecular qubits by quantum unitary spin dynamics. *J. Magn. Magn. Mater.* **487**, 165325 (2019).

[51] J. Chen, C. Hu, J. F. Stanton, S. Hill, H.-Ping Cheng, X.-Guang Zhang, Decoherence in Molecular Electron Spin Qubits: Insights from Quantum Many-Body Simulations. *J. Phys. Chem. Lett.* **11**, 2074–2078 (2020).

[52] E. R. Canarie, S. M. Jahn, S. Stoll, Quantitative Structure-Based Prediction of Electron Spin Decoherence in Organic Radicals. *J. Phys. Chem. Lett.* **11**, 3396–3400 (2020).

[53] S. Kanai, F. J. Heremans, H. Seo, H. Ohno, Generalized scaling of spin qubit coherence in over 12,000 host materials. *Proc. Natl. Acad. Sci. U.S.A* **119**, 15 (2022).

[54] X.-Fa Jiang, Z.-Bo Hu, C. Shao, Z. Ouyang, Z. Wang, Y. Song, Molecular Spin Qubits Impregnated in a Hexagonal Self-Ordered Mesoporous Silica. *Chem. Mater.* **34**, 8427–8436 (2022).

[55] K. Kundu, J. Chen, S. Hoffman, J. Marbey, D. Komijani, Y. Duan, A. Gaita-Ariño, J. Stanton, X. Zhang, H.-Ping Cheng, S. Hill, Electron-nuclear decoupling at a spin clock transition. *Commun. Phys.* **6**, 38 (2023).

[56] A. Lunghi, F. Totti, R. Sessoli, S. Sanvito, The role of anharmonic phonons in under-barrier spin relaxation of single molecule magnets. *Nat. Commun.* **8**, 14620 (2017).

[57] L. Escalera-Moreno, J. J. Baldoví, A. Gaita-Ariño, E. Coronado, Spin states, vibrations and spin relaxation in molecular nanomagnets and spin qubits: a critical perspective. *Chem. Sci.* **9**, 3265-3275 (2018).

[58] A. Lunghi, S. Sanvito, How do phonons relax molecular spins? *Sci. Adv.* **5**, 9 (2019).

[59] M. Briganti, F. Santanni, L. Tesi, F. Totti, R. Sessoli, A. Lunghi, A Complete Ab Initio View of Orbach and Raman Spin–Lattice Relaxation in a Dysprosium Coordination Compound. *J. Am. Chem. Soc.* **143**, 13633–13645 (2021).

[60] D. Reta, J. G. C. Kragskow, N. F. Chilton, Ab Initio Prediction of High-Temperature Magnetic Relaxation Rates in Single-Molecule Magnets. *J. Am. Chem. Soc.* **143**, 5943–5950 (2021).

[61] A. Lunghi, Toward exact predictions of spin-phonon relaxation times: An ab initio implementation of open quantum systems theory. *Sci. Adv.* **8**, 31 (2022).

[62] S. Mondal, A. Lunghi, Unraveling the Contributions to Spin–Lattice Relaxation in Kramers Single-Molecule Magnets. *J. Am. Chem. Soc.* **144**, 22965–22975 (2022).

[63] P. Szańkowski, Introduction to the theory of open quantum systems. ArXiv 2209.10928v1 (2022).

[64] A. Norambuena, E. Muñoz, H. T. Dinani, A. Jarmola, P. Maletinsky, D. Budker, J. R. Maze, Spin-lattice relaxation of individual solid-state spins. *Phys. Rev. B* **97**, 094304 (2018).

[65] J. E. Avron, O. Kenneth, A. Retzker, M. Shalyt, Lindbladians for controlled stochastic Hamiltonians. *New J. Phys.* **17**, 043009 (2015).

[66] M. Atzori, E. Morra, L. Tesi, A. Albino, M. Chiesa, L. Sorace, R. Sessoli, Quantum Coherence Times Enhancement in Vanadium(IV)-based Potential Molecular Qubits: the Key Role of the Vanadyl Moiety. *J. Am. Chem. Soc.* **138**, 11234–11244 (2016).

[67] M. Atzori, L. Tesi, E. Morra, M. Chiesa, L. Sorace, R. Sessoli, Room-Temperature Quantum Coherence and Rabi Oscillations in Vanadyl Phthalocyanine: Toward Multifunctional Molecular Spin Qubits. *J. Am. Chem. Soc.* **138**, 2154–2157 (2016).

[68] K. Bader, D. Dengler, S. Lenz, B. Endeward, S.-Da Jiang, P. Neugebauer, J. van Slageren, Room temperature quantum coherence in a potential molecular qubit. *Nat. Commun.* **5**, 5304 (2014).

[69] Y. Dai, Z. Shi, Y. Fu, X. Qin, S. Mu, Y. Wu, J.-Hu Su, L. Qin, Y.-Qi Zhai, Y.-Fei Deng, X. Rong, J. Du, Experimental protection of the coherence of a molecular qubit exceeding a millisecond. arXiv:1706.09259 (2017).

[70] L. Escalera-Moreno, N. Suaud, A. Gaita-Ariño, E. Coronado, Determining Key Local Vibrations in the Relaxation of Molecular Spin Qubits and Single-Molecule Magnets. *J. Phys. Chem. Lett.* **8**, 1695–1700 (2017).

[71] A. Lunghi, F. Totti, S. Sanvito, R. Sessoli, Intra-molecular origin of the spin-phonon coupling in slow-relaxing molecular magnets. *Chem. Sci.* **8**, 6051-6059 (2017).

[72] A. Lunghi, S. Sanvito, The Limit of Spin Lifetime in Solid-State Electronic Spins. *J. Phys. Chem. Lett.* **11**, 6273–6278 (2020).

[73] V. H. A. Nguyen, A. Lunghi, Predicting tensorial molecular properties with equivariant machine learning models. *Phys. Rev. B* **105**, 165131 (2022).

[74] S. Lenz, B. Kern, M. Schneider, J. van Slageren, Measurement of quantum coherence in thin films of molecular quantum bits without post-processing. *Chem. Commun.* **55**, 7163-7166 (2019).

[75] A. Albino, S. Benci, L. Tesi, M. Atzori, R. Torre, S. Sanvito, R. Sessoli, A. Lunghi, First-Principles Investigation of Spin–Phonon Coupling in Vanadium-Based Molecular Spin Quantum Bits. *Inorg. Chem.* **58**, 10260–10268 (2019).

[76] M. J. Amdur, K. R. Mullin, M. J. Waters, D. Puggioni, M. K. Wojnar, M. Gu, L. Sun, P. H. Oyala, J. M. Rondinelli, D. E. Freedman, Chemical control of spin–lattice relaxation to discover a room temperature molecular qubit. *Chem. Sci.* **13**, 7034-7045 (2022).

[77] L. Gu, J. Li, R. Wu, Reconsidering spin-phonon relaxation in magnetic molecules. *J. Magn. Magn. Mater.* **564**, 170138 (2022).

[78] M. Shiddiq, D. Komijani, Y. Duan, A. Gaita-Ariño, E. Coronado, S. Hill, Enhancing coherence in molecular spin qubits via atomic clock transitions. *Nature* **531**, 348–351 (2016).

[79] T. Abad, A. F. Kockum, G. Johansson, Impact of decoherence on the fidelity of quantum gates leaving the computational subspace. arXiv:2302.13885 (2022).

[80] J. Liu, J. Mrozek, A. Ullah, Y. Duan, J. J. Baldoví, E. Coronado, A. Gaita-Ariño, A. Ardavan, Quantum coherent spin–electric control in a molecular nanomagnet at clock transitions. *Nat. Phys.* **17**, 1205–1209 (2021).